Advanced Nanostructured Electrode and Materials Design for Zinc Air Batteries

by

Jordan Scott

A thesis

presented to the University of Waterloo

in fulfillment of the

thesis requirement for the degree of

Master of Applied Science

in

Chemical Engineering

Waterloo, Ontario, Canada, 2013

Authors Declaration

I hereby declare that I am the sole author of this thesis. This is a true copy of the thesis, including any required final revisions as accepted by my examiners.

I understand that my thesis may be made electronically available to the public.

Abstract

Zinc air batteries have great promise as a new age energy storage device due to their environmental benignity, high energy density in terms of both mass and volume, and low cost Zinc air batteries get their high energy density by using oxygen from the air as the active material. This means that all the mass and volume that are normally required for active material in a battery are replaced by a thin gas diffusion electrode which allows for oxygen from the air to diffuse into the cell. Although this seems ideal, there are many technical challenges associated with the cell being open to the atmosphere. Some of these issues include electrolyte and electrode drying out, poor reaction kinetics involving sluggish reaction, the need for bifunctional catalysts to charge and discharge, and durability of the gas diffusion electrode itself.

The bifuntional catalysts used in these systems are often platinum or other precious metals since these are commonly known to have the highest performance, however the inherent cost of these materials limits the feasibility of zinc air systems. Thus, there is a need to limit or remove the necessity for platinum carbon catalysts. There are many types of non precious metal catalysts which can be used in place of platinum, however their performance is often not as high, and the durability of these catalysts is also weak. Similar limitations on feasibility are invoked by the poor durability of the gas diffusion electrodes. Carbon corrosion occurs at the harsh caustic conditions present at the gas diffusion electrodes, and this corrosion causes catalyst dissolution. Moreover, many issues with zinc electrode fabrication limit durability and usable anode surface area within these systems. There is a need for a stable, porous, high surface area anode with good structural integrity. These issues are addressed in this work by three studies which each focuses on solving some of the issues pertaining to a crucial component of zinc air batteries, those being

the gas diffusion electrode, the zinc electrode, and the bifunctional catalyst necessary for oxygen reduction reactions (ORR) and oxygen evolution reactions (OER).

The first study addresses the need for improvements to the zinc anode electrode. A new process is proposed for the production of porous zinc electrodes in which the porosity can be easily controlled. This process involves the mixing of atomized zinc powder with a filler compound such as ammonium chloride. The mixture is then pressed into a pellet and heat treated to a temperature which simultaneously sublimes/decomposes the filler compound, and anneals the zinc structure to improve structural integrity. The resultant porous anode showed significantly charge and discharge potentials over the solid plate anode, while allowing for increased control of porosity over other porous electrodes due to the ability to adjust pore size based on the filler compound particle size. The discharge potentials observed from these porous anodes were 20% greater than zinc plate anodes at 100mA, but up to 200% greater at elevated currents of 200mA. Similarly the charging potentials were 53.8% lower at 100mA, and 55.5% lower at 200mA., suggesting greatly improved performance by the porous anode.

The second study addresses the need for more durable gas diffusion electrodes. In this study, the bifunctional catalyst was bound directly to a stainless steel current collector via polymer binding in an attempt to remove the possibility of carbon corrosion and catalyst dissolution. The new gas diffusion electrode was successful in eliminating carbon corrosion, wherein, the durability of cells which incorporate this type of electrode was significantly increased. The durability of cell was increased to a point where little to no degradation occurred over 1000 cycles of full cell testing, showing great promise for future use and commercial viability.

The final study addresses the need for durable and high performance non precious metal catalysts. The effects of catalyst morphology were studied wherein various morphologies of spinel type cobalt oxide were synthesized and compared. Cobalt oxide nanosheets were successfully synthesized and compared to nanoparticles of comparable size. The cobalt oxide nanosheets showed better charge and discharge potentials as well as durability of the nanoparticles. Impedance analyses showed reduced charge transfer and cell component resistances associated with the nanosheet morphology. Cobalt oxide nanosheets were further compared against platinum carbon. Cobalt oxide nanosheets showed significantly better durability as well as lower charging potentials and higher discharge potentials over 75 cycles. After 75 cycles the platinum carbon had lost 55.7% of its discharge potential wherein cobalt oxide nanosheets lost none of its discharge potential.

Three issues pertaining to three major cell components a zinc air were addressed with promising solutions proposed for each. This work provides a basis for advanced zinc electrode fabrication in which further improvements can be incorporated to address other issues pertaining to zinc electrode use. This work set up a basis for electrode design which focuses on non carbon supported catalysts, eliminating the issue of carbon corrosion and associated catalyst dissolution. Finally, the results from the morphology study elucidate the benefits of controlled morphology for bifunctional catalysts, showing how morphology can be adjusted to improve performance by improving cell and charge transfer resistances.

Acknowledgements

Special thanks goes to my supervisor, Dr. Zhongwei Chen and several of my colleagues including Jason Wu, Zhu Chen, Fathy Hassan, Drew Higgins, and Dong Un Lee for their assistance.

I would like to acknowledge support from my reviewers, including Dr. Zhongwei Chen, Dr. Aiping Yu, and Dr. Michael Fowler.

Contents

List of Figures

List of Tables

List of Abbreviations, Symbols, and Nomenclature

CV	cyclic voltammertry
EDAX	energy dispersive x-ray spectroscopy
E°	standard reversible redox potential
e^-	electron
GDL	gas diffusion layer
ORR	oxygen reduction reaction
OER	oxygen evolution reaction
Pt/C	carbon support platinum nanoparticles
PTFE	polytetraflouroethylene
RRDE	rotating ring disk electrode
SEM	scanning electron microscopy
TEM	transmission electron microscopy
XRD	x-ray diffraction

Introduction

1.1 The growing Energy Problem

There is a growing energy challenge associated with our society's dependence on fossil fuels. With fossil fuels, a non-renewable resource, making up the vast majority of our energy use especially in the transportation sector, society is left will few options as to combat rising oil prices and depleting reserves. It is estimated that conventional oil production will peak by 2020 [1], leaving society to focus on more expensive methods of acquiring oil through unconventional reserves. This rise in oil price and dependence on fossil fuel use greatly affects the transportation sector, where few but growing numbers of electric and hybrid electric vehicles are being introduced. The use of hybrid vehicles and electric vehicles have many advantages, with one of the most major being their fuel source is unspecific, allowing them to run on electricity generated either by nuclear, renewable, or fossil fuels. Additionally the burning of the fossil fuels external to cities is extremely beneficial to the health of the population. Smog and poor air quality can cause health effects on individuals.

Lithium ion batteries are currently the battery chemistry of choice for these electric and hybrid vehicle applications. Rechargeable lithium ion batteries differ from non rechargeable variations mainly due to the intercalated lithium compound that is used, which allows for recharging. There are many advantages to the use of lithium ion batteries, include the lack of "memory effect", extremely low self discharge rates, and environmental benignity. However, with these advantages come a slew of disadvantages. Cell life is noticeably lower compared to other battery chemistries, especially when kept at full charge. The cell life degradation can be significantly

reduced if kept around half charged, but this does not always fit well to applications. Additionally there are safety concerns associated with the use of lithium ion batteries and their potential for thermal runaway. This can require a large amount of safety features required in each cell, which can cause increase the manufacturing cost. Finally, the price of lithium ion batteries is quite high and even with recent advancements the price of lithium ion batteries are not expected to fall below $500/KWh [2]. This is in part due to the manufacturing requirements of atmospheres which contain no water. Water can react with the lithium present and ruin the battery. Furthermore, with the need for extended ranges in electric and hybrid vehicles, and the need to incorporate more of these vehicles into society, there is a strong need for a battery which not only has a much higher energy density, but one which is safer, and much cheaper.

Zinc air batteries present an opportunity here, wherein there inherent energy density is theoretically up to five times that of lithium ion. Additionally zinc air batteries require no specific manufacturing environments, and have no chance of thermal runaway. Most interesting of all is the extremely low cost of zinc air batteries, where the anodic material, zinc, is extremely abundant and already used commercial for many applications pertaining to corrosion resistance. Zinc is the 4^{th} most produced metal in the world and is extremely cheap [2]. However, there are also many issues with the current technology in zinc air batteries. The main issues with zinc air batteries are there low cell life and the difficulty in cycling or recharging the cell. It can be noted that for platinum/carbon on a carbon gas diffusion layer, it only requires 100 cycles before the discharge potential is 50% of the initial [3]. Thus, this thesis is directed at solving these issues. This thesis will focus on improving cell life, while simultaneously improving the charge and discharge potentials required for performance. The report is structured so that the reader will have a specific understanding of the technical challenges and drawbacks associated with zinc air

battery technologies pertaining to many aspects of the battery. In each section the technical challenges will be outlined along with the proposed design solution. The experimental design specifics associated with each subsequent study will be discussed, followed by analysis of the results obtained during preliminary testing of these designs. Three separate designs and investigations were carried out, each focused on a different integral part of zinc air batteries. These designs pertain to the cathode, anode, and bifunctional catalyst used. These sections involve:

i. A new single heat treatment method for producing controlled porosity zinc anodes;

ii. Advanced cathodic electrode design pertaining to replacing carbon and avoiding carbon corrosion; and,

iii. The effects of morphology on spinel cobalt oxide; a comparison of cobalt oxide nanoparticles and nanosheets.

Each of these three sections focuses on the improvement of durability, charging potential, discharging potential, or a combination of those herein.

1.2 Zinc Air Batteries

Zinc air batteries are a promising battery chemistry which takes advantage of the use of oxygen present in the air as a source of oxidizing agent. Zinc air batteries have significantly higher energy density than competing battery chemistries for this reason. Where normally a solid fuel would be required to produce the required oxidation and reduction reactions required for current generation, zinc air batteries use the oxygen in the air, significantly reducing the mass of and

volume of the battery required. It can be seen in Fig. 1 that zinc air remains the furthest progressed along a relationship comparing volumetric and mass energy densities. Based on mass energy density, it can be seen that zinc air can practically have between two and three times the energy density of currently used lithium ion batteries. Similarly so, a significant improvement in volumetric energy density can be seen as zinc air has the potential for improvements by as much as 50%.

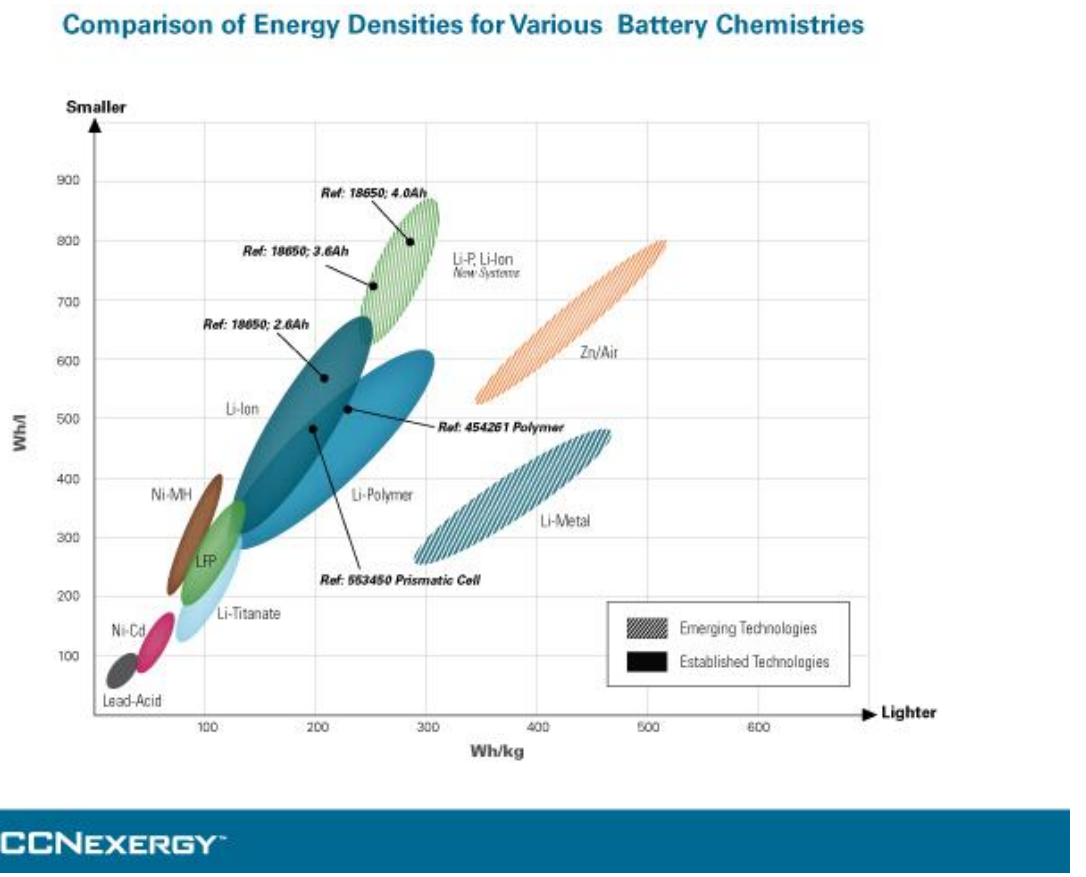

Figure 1: A comparison of battery chemistry and specific energy densities based on mass and volume respectively [4].

Zinc air batteries also have many advantages over other types of metal air batteries, for example lithium air batteries, which have a higher theoretical energy density, but lack practicality at their current stage of development. Lithium air batteries have many issues pertaining to scalable

manufacture due to the issues associated with handling lithium, as well as safety concerns. Issues also arise with durability, wherein lithium air batteries have poor retention of capacity [5-11]. Zinc metal has an electrochemical equivalent density of $0.82 Ahg^{-1}$ and is extremely electropositive, which is advantageous to electrodeposition associated with charging [5, 12-14]. The high electro positivity, low cost, and environmentally benignity of zinc makes it an ideal material for use in energy storage.

Zinc air batteries function similarly to other batteries in the sense that they have two electrodes, one solid zinc electrode which functions primarily as the anode during discharge, and one air breathing electrode which allows the diffusion of air into the cell. The electrodes may be separated by a separator membrane which is used to prevent particulate transfer from one electrode to the other. The membrane can be treated to also prevent zinc hydroxide and zinc ion transfer to the cathodic side of the cell. This can aid to prevent short circuiting in cells which undergo a significant amount of cycling. The electrochemical reactions required for zinc air battery function are as follows.

Anodic Reactions:

1) $Zn \rightarrow Zn^{2+} + 2e^-$

2) $Zn^{2+} + 4OH^- \rightarrow Zn(OH)_4^{2-}$

(Eo = − 1.25 V NHE)

or

3) $Zn(OH)_4^{2-} \rightarrow ZnO + H2O + 2OH^-$

4) $Zn + 2H_2O \rightarrow Zn(OH)_2 + H_{2(g)}$

Illustration of these reactions can be viewed in Fig. 2.

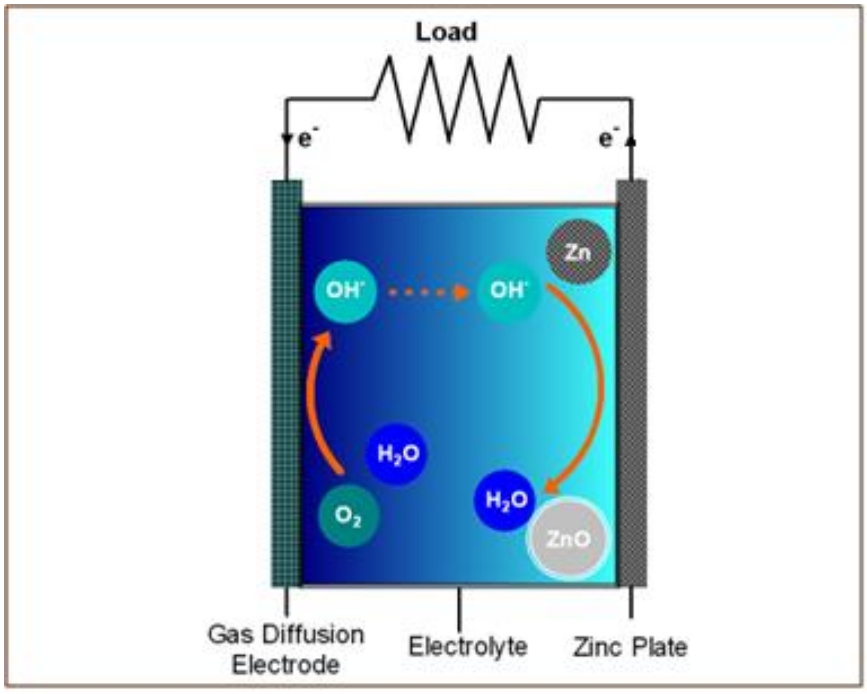

Figure 2: Schematic of zinc air battery function [4]

Reactions 1 and 2 show the standard reaction which occur in order to generate current. These reactions take place in alkaline conditions, often, at least in this work, in conditions at or more alkaline than pH 12. Upon discharge, hydroxyl ions in solution react with zinc ions and produce two electrons, as seen by equation 2. Reactions 3 and 4 are side reactions which can occur and are often detrimental to cell performance. As the solution becomes significantly more saturated with zincate ions, due to repeated cycling of the cell, side reaction 3 can be seen wherein excess zincate reacts to form zinc oxide. Reaction 4 can be observed at the over potentials in the cell. Zinc metal reacts with water at elevated potentials to form hydrogen gas. This hydrogen evolution occurs specifically during charging, wherein the cell is forced under high potentials to charge the battery.

Oxygen is allowed to continuously diffuse through the air breathing electrode and react with the bifunctional catalyst in the cathodic electrode. There are two different pathways in which

hydroxyl ions can be produce at the air cathode, a four electron pathway and a two electron pathway. The more advantageous and efficient pathway is the 4-electron pathway. Oxygen and two water molecules react to produce for hydroxide ions and use up four electrons, hence the four electron pathway.

5) $O_2 + 2H_2O + 4e^- \rightarrow 4OH^-$

($E° = 0.4\ V_{NHE}$)

The two electron pathway instead involves the reaction of oxygen with a single water molecule, producing hydroperoxide and a single hydroxide ion while using only two electrons. A second reaction then occurs where the hydroperoxide further reacts with another water molecule to produce three more hydroxyl ions and uses up two more electrons. Overall, both reaction pathways use 4 electrons, however the difference in over potentials required make the four electron path way much more desirable. This is because a higher potential is required for charging with the two electron pathway, wherein hydrogen evolution is more likely to occur, and charging efficiency is reduced. The two reactions of the two electron pathway are as follows.

6) $O_2 + H_2O + 2e^- \rightarrow HO_2^-\ OH^-$

($E° = -0.065V_{NHE}$)

7) $HO_2^- + H_2O + 2e^- \rightarrow 3OH^-$

($Eo = 0.867V_{NHE}$)

By comparison the E° for the four electron pathway is 0.4 V_{NHE} while the E° for the hydroperoxide reaction with water is 0.867V $_{NHE}$. Overall the reaction involves the oxidation of zinc metal to zinc oxide.

Overall Reaction:

$2Zn + O_2 \rightarrow 2ZnO$

($E° = 1.65$ V)

However, the cathodic reactions are extremely sluggish. For this reason catalyst are required to increase the reaction rates to viable speeds for practical use. The most sensible solution is to incorporate bifunctional catalysts into the gas diffusion electrode which promotes both the forward and reverse cathodic reactions, which are required for charge and discharge. These reactions furthermore labeled as the oxygen evolution (charging) reaction, and the oxygen reduction (discharge) reaction. Precious metals currently are some of the best performing oxygen reduction (ORR) and oxygen evolution (OER) catalysts, however there scarcity and high cost limit their usefulness in zinc air systems. There is a large demand for well performing non-precious bifunctional catalysts. There are a plethora of non precious catalysts which are emerging technologies hoping to outperform platinum. For example, some carbon based possible ORR catalysts include nitrogen doped carbon nanotubes [15], nitrogen doped carbon nanocapsules [16], grapheme carbon nitride [17], nitrogen doped carbon [18], and iron plthalocyanine [19]. A lot of focus has been spent on nitrogen doping of carbon based catalyst to greatly improve catalytic activity, while the carbon structure allows for good conductivity within the catalyst. These catalysts have adequate performance but can lack in durability and OER performance. One of the solutions to this is spinel and perovskite type catalysts. Some examples of non-precious, metal oxide based catalysts include Mn_3O_4/rGraphine Oxide [20], $CoMn_2O_4$ [21], and Mn_3O_4 [22]. Unfortunately, metal oxides have very poor conductivity, with this being a major contributor to increased cell impedance and resistance values, inhibiting performance. A variety of substrates have been incorporated into the active catalyst layer to try and overcome this lack of conductivity [23-26]. Similarly to how there are a multitude of catalyst compositions,

there are also a number of catalyst morphologies, each with associated advantages and disadvantages pertaining to certain compositions. A variety of morphologies can be view below in Fig. 3-9 including nanospheres, nanofibre coated wires, nanowires, nanoflowers, nanoparticles, grapheme sheets, and composite materials.

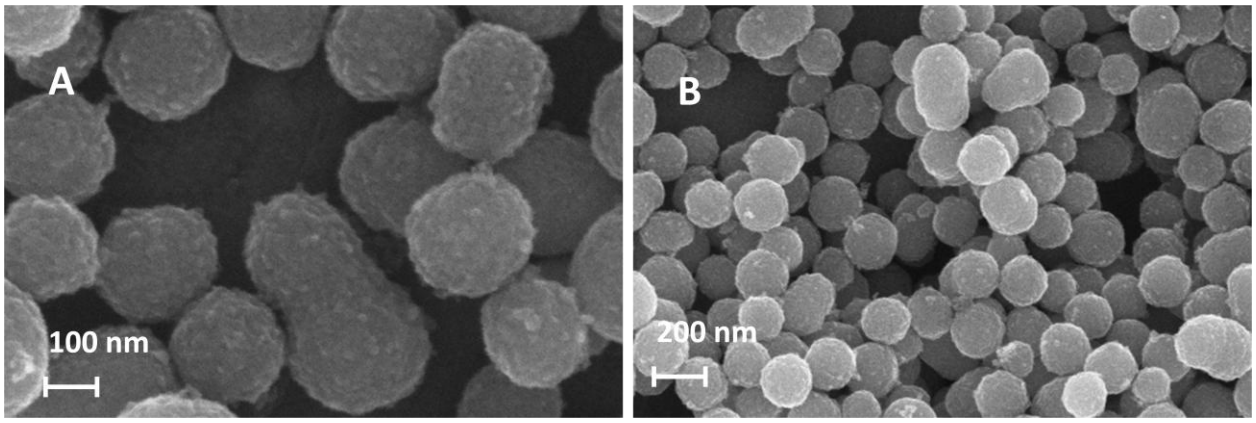

Figure 3: SEM images showing nanosphere morphology

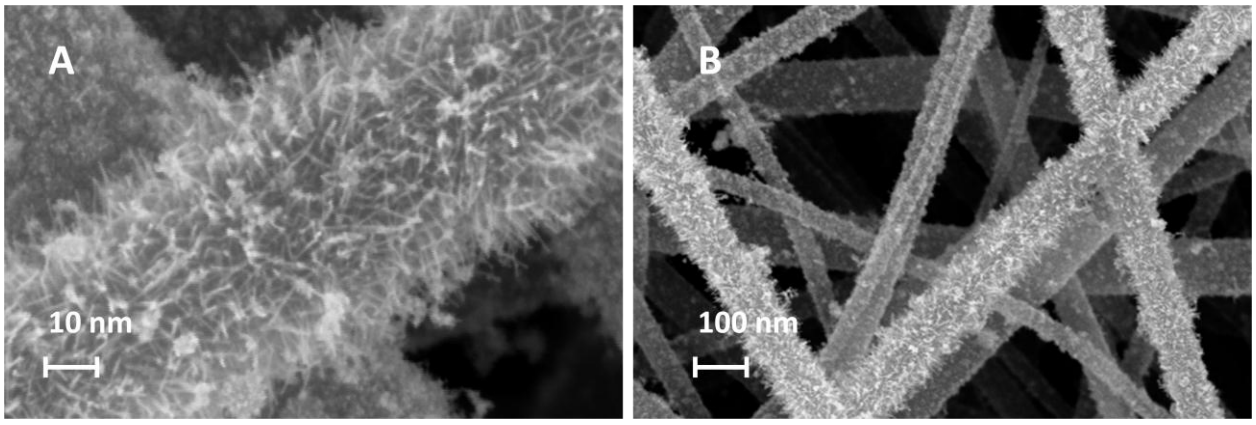

Figure 4: SEM images showing nanofibre coated wire morphology

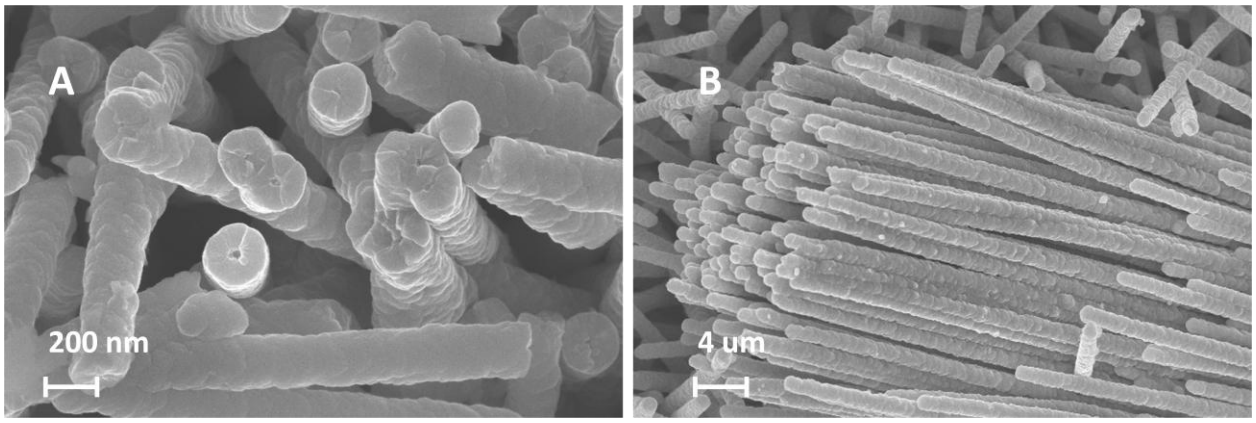

Figure 5: SEM images showing nanowire morphology

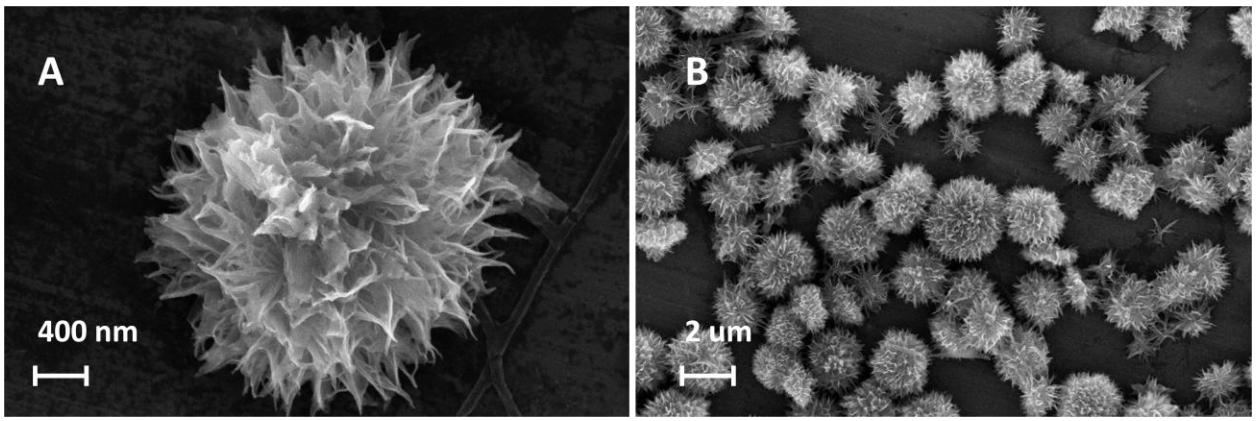

Figure 6: SEM images showing nanoflower morphology

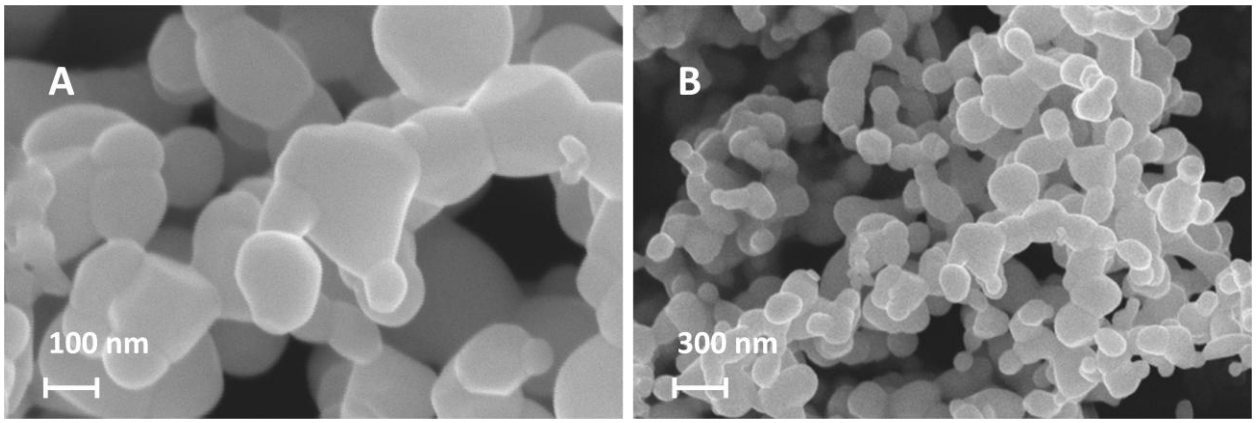

Figure 7: SEM images showing nanoparticle morphology

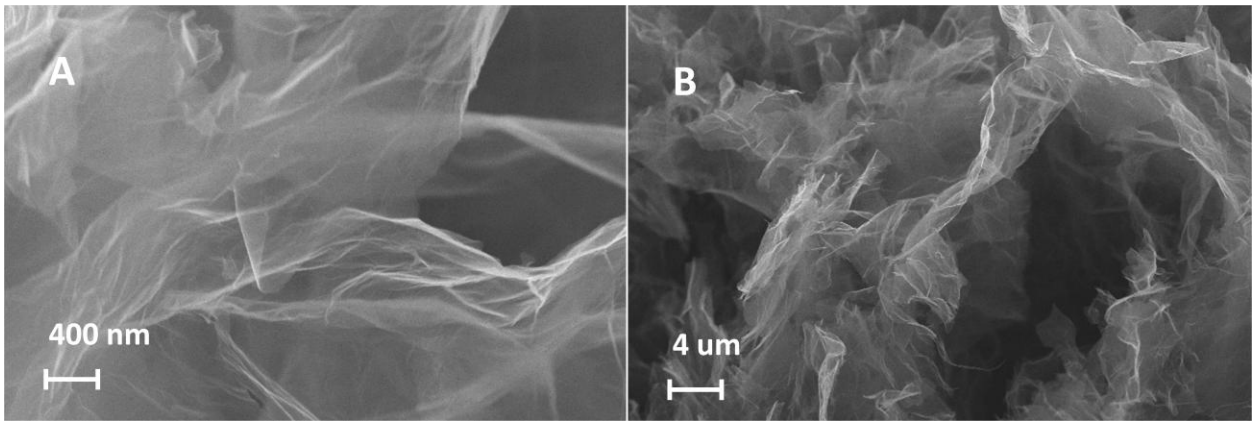

Figure 8: SEM images showing graphene sheet morphology

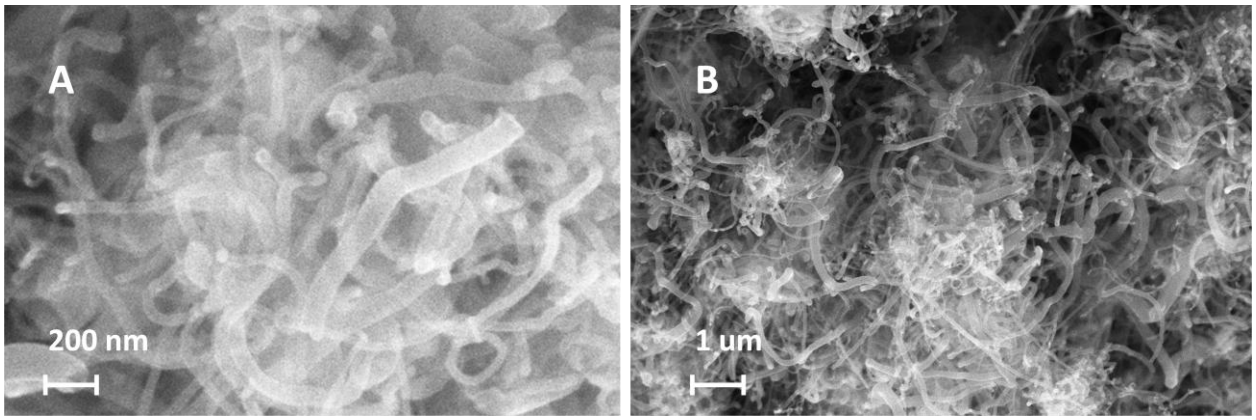

Figure 9: SEM images showing composite carbon nanotube and metal oxide nanowire morphology

1.2.2 Technical Challenges with Zinc Anode Electrode

The zinc electrode present in zinc air batteries is the main fuel source for the reaction. As such, exposed surface area at the anode of the battery can significantly influence battery performance. Bluntly put, higher surface area at the anode allows for easier reaction involving zinc, and translates to an increase in performance [10]. There are many factors which affect the overall battery performance, and of those, the most important factors pertaining to the anode are specific surface area, effective surface area, surface activity, porosity, electrical conductivity, and

mechanical stability [27]. A number of various morphologies of zinc electrodes have been tested, each with its own associated disadvantages. Zinc powder anodes are extremely popular due to their ease of fabrication and low cost. Zinc powder electrodes often consisted of atomized or micro sized zinc powder held together by a gelling agent to attempt to keep high contact between particles necessary for good conductivity of the anode [27]. Poor conductivity is one of the main disadvantages associated with gelled powder zinc anodes. Since there is no supporting structure behind the anode, each particle is free to move, and this results in particle which are completely separate or in minimal contact with the anode system. Additionally, as discharge continues the zinc particles shrink as zinc is used up in the anodic reactions. This shrinkage further separates particles and reduces conductivity. This leads to issues with durability and long cycle discharges. Typical porosity for zinc powder in alkaline batteries is between 50 and 58% [27]. Porosity is often limited in cell by the amount of gelling, where a higher amount gelling translates to higher porosity, but poorer conductivity. Zinc anodes formed by the gelling method also lack significantly in terms of structural integrity. The anode by design is not connected and is similar to a gel or paste. By this design it is easily torn or damaged by physical stimulation. For this reason, zinc powder is mainly used in primary zinc air batteries where no charging cycle is necessary, and where the battery is encased in solid nonflexible shell. However, even this does not solve all issues, since with too much porosity the electrical conductance of the cell can be unstable, and performance is sensitive to mechanical vibrations and movement [28]. Zinc dendrites are an attempt to improve upon the surface area and connectivity of porous electrodes, and are formed by the crystalline deposition of zinc ions. In normal zinc air function, the formation of dendrites is significantly detrimental to battery performance, due to inherent sharpness of the dendrite structure. Often, the dendrites from protruding perpendicular to the zinc

anode surface, and by doing so puncture the separator membrane of the cell. However, if this is accounted for in cell design, by designated enough distance between the anode and the separator membrane, zinc dendrites can be an effective anode do to the significantly improved surface area compared to zinc particles. Zinc dendrites are indeed and improvement over atomized powder, but they do not solve the mechanical stability and electrical conductivity associated with these particles type anodes. These structures are visible in Fig. 10.

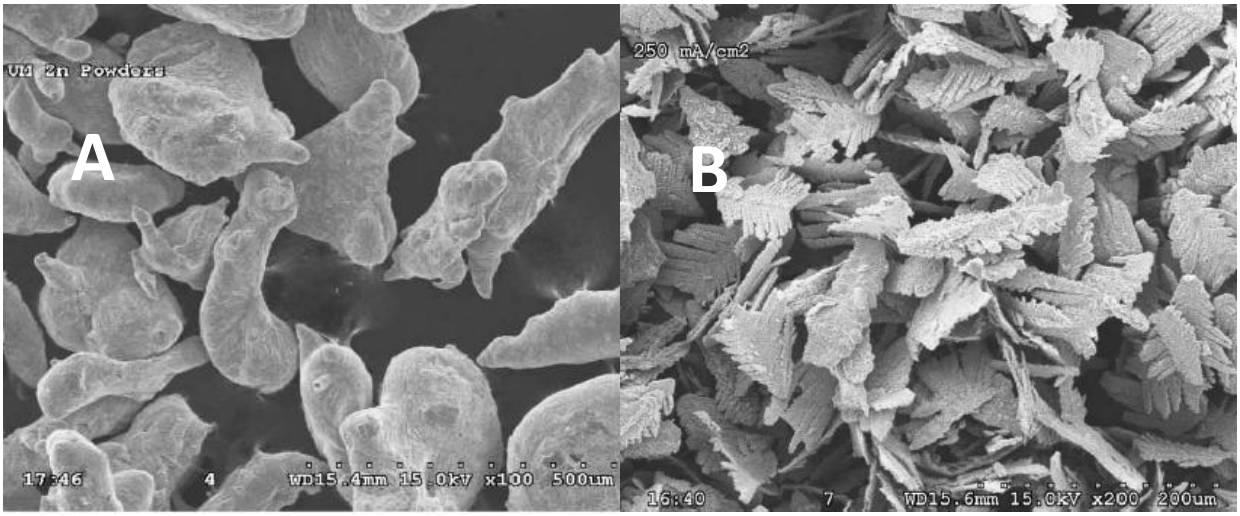

Figure 10: Comparison of atomized and dendrite zinc particulates structure [10]

One such solution to the interconnectivity and electrical conductance issues was the development of fibrous zinc anodes. These anodes were comprised of fibres spun off molten zinc and bundled together into a desired anode shape. These structures demonstrated significantly improved conductivity over both atomized zinc particles and dendritic zinc, however by theory it can be seen that during discharge, if zinc were to be used or eroded on two sides of a fibre, then that fiber would dislodge from the network and much of the connectivity from the lengthy fiber would be lost.

There are also many anode designs which instead focus on chemical or metallurgical improvements to anode materials rather than structural. Electrolyte additives such as phosphoric or citric acid can be added to significantly reduce dendrite formation [10]. This is essential to creating durable anodes which retain their initial structure design after significant cycling. It has been noted that additives not only reduce dendrite formation, but also increase the potential required for hydrogen evolution to occur.

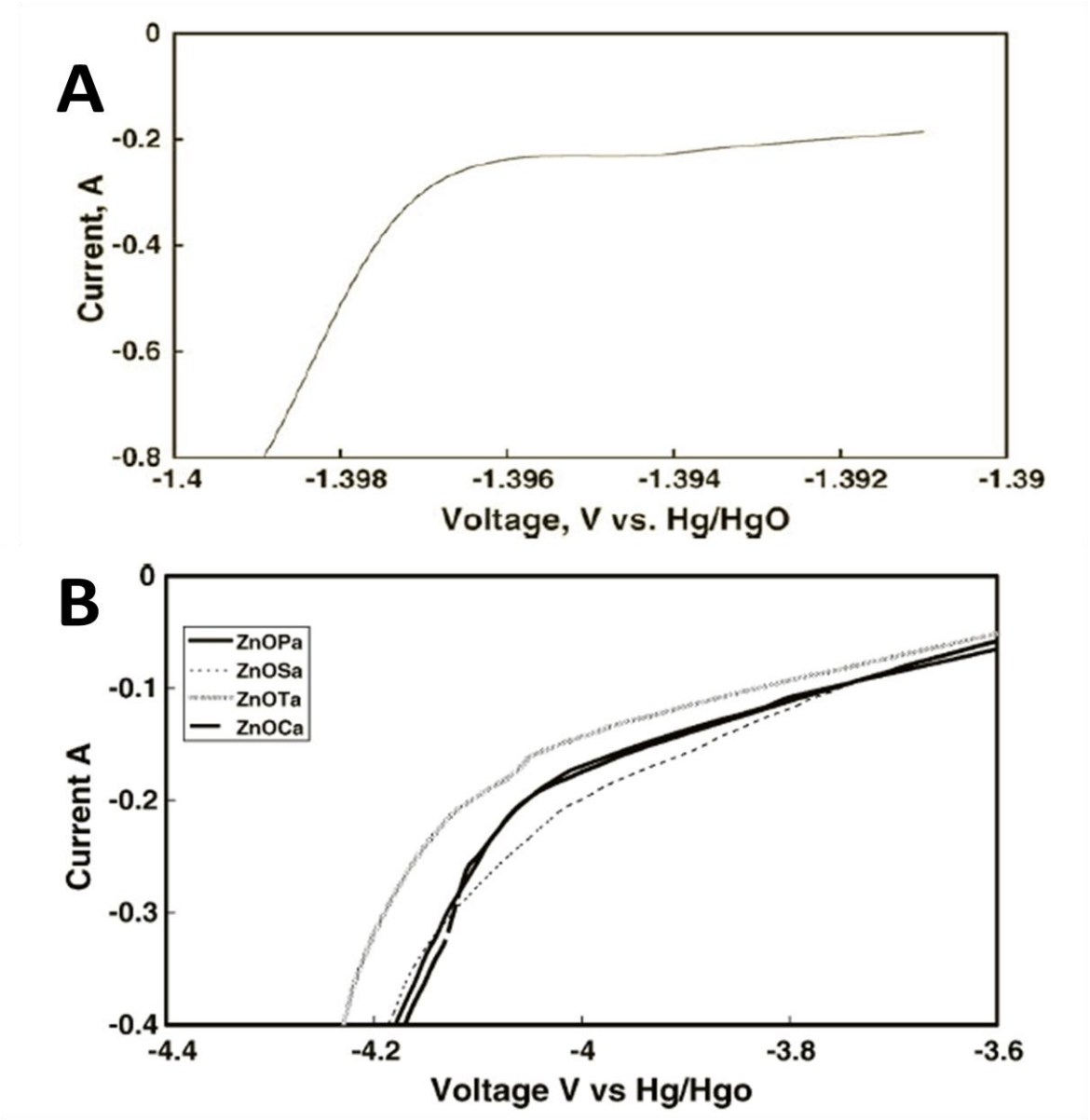

Figure 11: Comparison of potential versus Hg/Hgo for determining overpotential for hydrogen evolution. A) No electrolyte additives other than ethylene glycol, B) various electrolyte additives including, tartaric, succinic, phosphorous and citric acid, in addition to ethylene glycol [29]

As seen from Fig. 11, the over potential for hydrogen evolution was raised significantly to 4.1V, from 1.39V. This in turn indicates that if the charging potential for the zinc air cell can be kept below 4.1V, then no hydrogen evolutions should occur. Another method of controlling dendrite

formation was done by alloying the zinc with other metals such as nickel and indium [30]. This method was successful in reducing the dendrite formation as well as raising the hydrogen over potential, although not as significantly as with the electrolyte additives. While these methods do address some of the major issues associated with zinc electrodes, they do not address the major issues of poor anode connectivity, structural integrity, and poor porosity control. It would be extremely beneficial to developed a procedure for making porous zinc anodes which not only have improved structural integrity, but also improved conductivity, and ease of control over porosity.

1.2.3 Technical Challenges with Gas Diffusion Electrode

The gas diffusion electrode most commonly used for metal air batteries is very similar to that used in fuel cells. There is a carbon fiber based gas diffusion layer which is treated with polytetraflouroethylene (PTFE) to be hydrophobic. This hydrophobic carbon layer prevents electrolyte leakage while allowing oxygen diffusion into the cell via ambient air, as seen in Fig. 12. On either side of this gas diffusion layer, a mesh type current collector may be placed. Next a layer of high surface area carbon and catalyst combined to form an active catalyst layer, is added. The high surface area carbon has several functions including the addition of a hydrophilic layer to the electrode. This amorphous carbon layer aids in catalyst wetting and can create air pockets needed for the oxygen reduction reaction to take place.

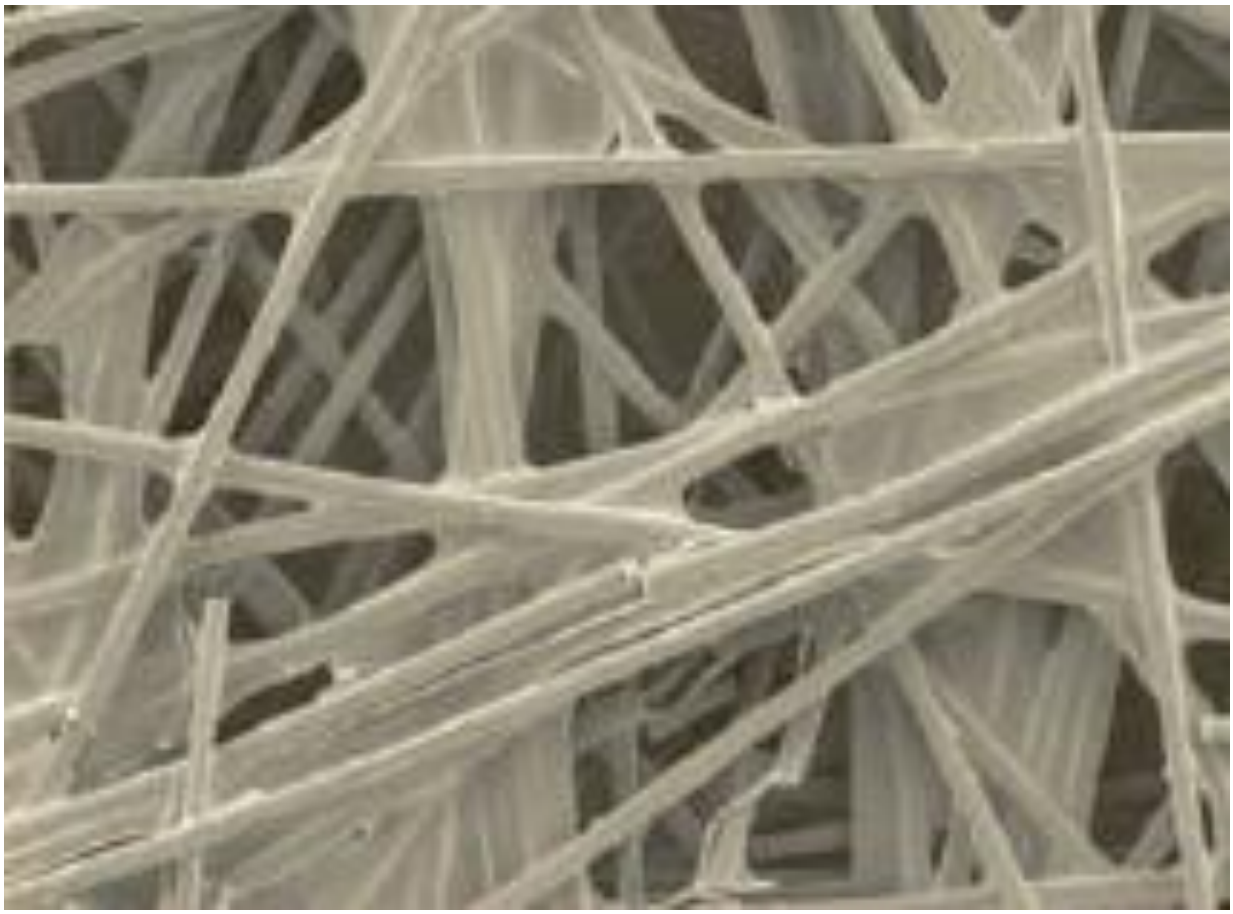

Figure 12: SEM of PTFE treated carbon fiber gas diffusion layer [31]

One major technical challenge associated with gas diffusion electrodes in both fuel cells and with metal air batteries is the corrosion of the carbon on which catalyst is loaded. During high potentials and in the presence of many harsh environments and operating conditions (such as open circuit voltage (OCV), be it caustic or acidic, the amorphous carbon corrodes, and the bifunctional catalyst responsible for oxygen reduction reaction (ORR) and OER reactions is subsequently lost from the electrode. This has been extensively observed with platinum loaded on carbon, and can also be seen through much testing of commercial primary catalyst responsible for oxygen reduction reactions. As seen through Fig. 13, after only 40 cycles there is a significant reduction in discharge and charge potentials. Manganese dioxide is extensively used

for long durations in primary batteries and is found to be quite stable for extended discharge periods [3]. It can be theorized that the rather quick degradation of full cell performance could be due to the loss of catalyst due to carbon corrosion. There is a need for an air electrode design which does not rely on the use of carbon for hydrophobicity and conductivity within the cell.

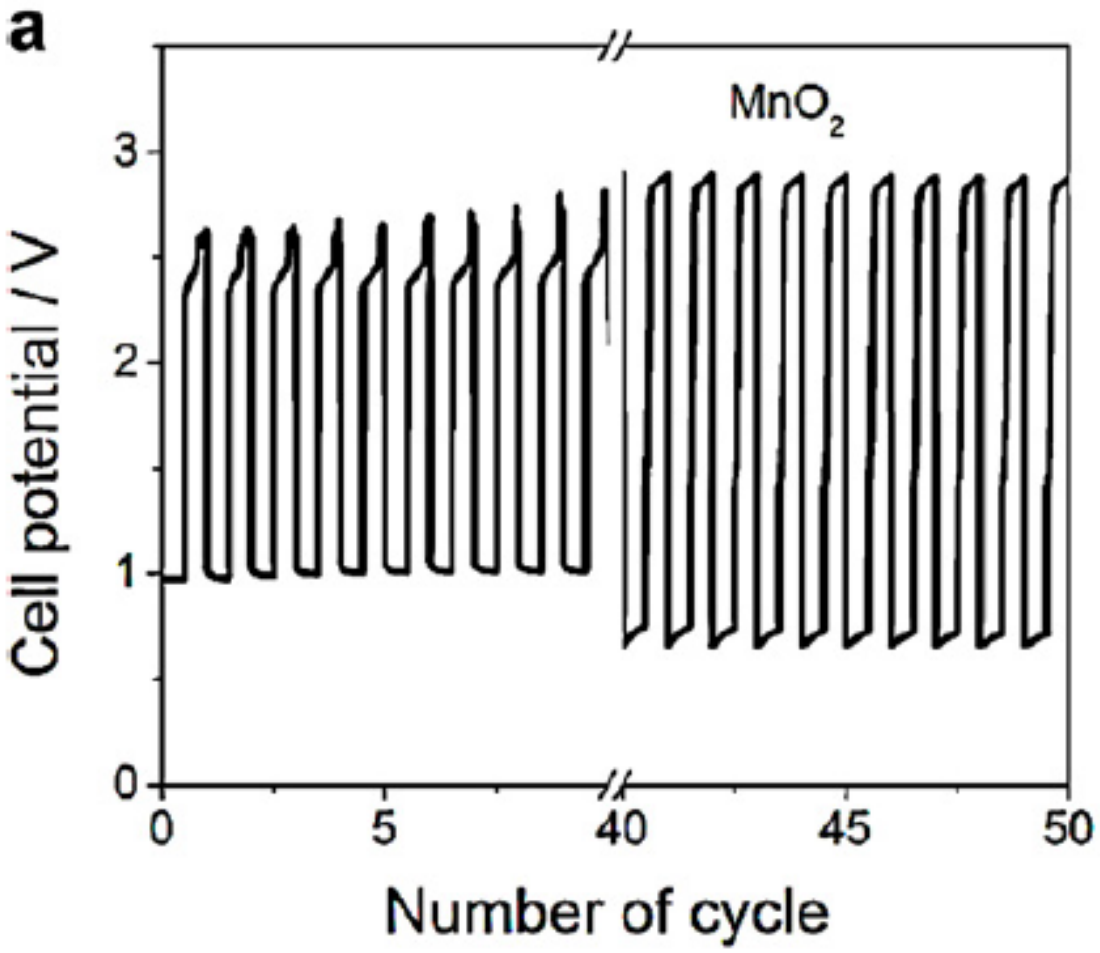

Figure 13: Charge and discharge cycling of manganese oxide load onto an amorphous carbon layer [3].

1.2.4 Technical Challenges with Bifunctional Cathode Catalysts

Currently, the most active bifunctional catalysts are unfortunately associated with or are solely precious metals. Platinum being the most active, while palladium and silver are also perform

quite well. The most durable and best performing catalysts are those of precious metals supported on amorphous high surface area carbon. However, the high cost and limited availability of platinum greatly hinders it use in zinc air batteries [31-33] A large number of catalystS are available and currently under investigation, many of these being transition metal oxides, perovskites, and spinel structured catalysts. The largest technical challenge associated with zinc air batteries viability is the lack of stable, durable, and high performance ORR and OER catalysts.

One of the most forefront, and still commercially used zinc air battery catalysts is MnO_2. Manganese oxide catalysts were used in the first ZAFC's [34], mainly due to its effectiveness for the oxygen reduction reactions associated with hydrogen peroxide decomposition by oxidation and reduction of surface manganese ions [34-36]. It has been noted that the morphology and fabrication method of manganese dioxide has a strong influence on performance [34,37]. Although manganese dioxide has strong ORR performance, and OER performance [34, 38-40], the durability of such compounds leaves much to be desired [3].

Another promising form of catalyst for ORR is silver based catalysts. Silver alone as an ORR catalyst cannot outperform catalysts such as platinum, however, when combined with carbides such as tungsten carbide, the half cell performance can at least equal that of platinum carbon [34, 41]. Similar to manganese oxide, the performance of silver based catalysts is attributed to the decomposition of hydrogen peroxide formed from the less desirable two electron pathway [34, 42].

Spinel type catalysts are metal oxide catalysts which follow the AB_2O_4 formula [34], where A is a divalent metal ion, B is a trivalent metal ion and O is oxygen. A and B do not need to be

different elements, just follow the need for trivalent and divalent variations. For example, cobalt has both trivalent and divalent variations of ions, and hence cobalt oxide in the spinel form Co_3O_4 is possible. Spinel type catalysts, specifically cobalt have reasonable promise as non precious catalysts, due to their ease of fabrication and low cost. Cobalt oxide in particular has good corrosion resistance in highly alkaline solutions, however, poor conductivity and relatively poor oxygen reduction capabilities. A list of non precious semiconducting oxides can be seen below.

Table 1: List of non precious semiconducting oxides and there comparative properties [34,42]

Oxide	Electrical Conductivity	Corrosion Resistance	Oxygen Reduction
La/La2O3	Poor	Good	Poor
Ti2O3/TiO2	Poor	Good	Poor
V2O4/V2O3	Poor	Poor	Poor
Cr2O3/CrO2	Poor	Poor	Poor
MoO2/MoO3	Poor	Poor	Poor
W2O3/WO3	Poor	Poor	Poor
Mn2O3/MnO2	Fair	Doubtful	Fair
Co2O3/CoO2	Poor	Good	Poor
Ni2O3/NiO2	Poor	Good	Poor
Cu2O/CuO	Poor	Doubtful	Good

It can be see then that although cobalt oxide has poor oxygen reduction capabilities and poor electrical conductivity; all stable and corrosion resistant non precious semiconducting oxides have these flaws. It would be extremely beneficial to develop a non precious metal bifunctional catalyst with good corrosion resistance, oxygen reduction capabilities and electrical conductivity. A catalyst with these properties would be suitable for use in zinc air batteries, due to the reduced cell impedance associated with good conductivity, the increased durability

associated with good corrosion resistance, and the reduced over potentials in improved performance associated with the ability to effectively carry out ORR.

1.4 Project Scope and Objectives

Overall the project may be divided into three main objectives, each dealing with a various portion of zinc air cell design.

1) The first project will deal with design and fabrication of electrodes, focused on the exclusion of carbon by design. Carbon corrosion has been seen to contribute to catalyst loss and poor durability in many cells. This can widely be seen across fields, even pertaining to platinum loading on carbon for use in fuel cells. The objective of the design is to remove unnecessary carbon aspects of the air breathing electrode design, specifically those which deal with adhesion of catalyst to the electrode, in order to substantially increase cell durability and performance.

2) The second project will entail a new fabrication process for porous zinc anode fabrication. In many systems, powder type zinc anodes are used. These powder type anodes have poor connectivity and conductivity due to the ease of separation of particles and void space formation during discharge. The objective entails the design of an economically feasible procedure for producing porous zinc anodes, which is simple, and ideally environmentally benign, since this is one of the advantages of zinc air batteries.

3) The third project will study the effects of bifunctional catalyst morphology on the full cell performance. More specifically, understanding the differences in impedance and

conductivity related performance between various morphologies of spinel type cobalt oxide. The study will investigate and compare full cell cycling performance of various morphologies these catalyst while comparing these performance to that of precious metal and alternative commercial catalysts.

Though these three projects, we can improve three major and integral parts of zinc air batteries, overcoming many technical challenges associated with zinc air battery use, and ideally bring the technology closer to commercial feasibility.

2.0 Structural and Electrochemical Characterization Techniques

2.1 Sample Preparation

The details of the sample preparation can be found in the following sections:

3.4.2 Preparation of porous zinc anode. This procedure utilized pressing a mixture of zinc and a filler compound to create a pellet. This pellet was further heat treated to produce porous anodes.

4.2.1 Preparation of gas diffusion cathode. This procedure utilized spray coating techniques as well as preparation of a catalyst ink. The full electrode design consists of an active catalyst layer which acts as the current collector, and a carbon gas diffusion layer

5.2.1 Preparation of the cobalt oxide nanosheets. This procedure utilized surfactants to control the Kelvin energy barrier of the particles formed, allowing for specific morphologies to arise. Autoclave hydrothermal synthesis as well as calcination in a tube furnace is incorporated into the procedure.

2.2 Scanning Electron Microscopy

The need for more powerful microscopes was prominently addressed by Manfred Von Ardenne in 1937 with the invention of a true microscope which utilized the signals from electron interactions to derive images at extremely high magnifications. The scanning electron microscope (SEM) plays an important role in the materials science field today, and is essential in understanding materials composition and topography. The microscope functions by scanning a

sample with a concentrated beam of electrons, and based on the reactions of these electrons with those of the sample, an image can be constituted, revealing important information regarding the surface of materials. The microscope functions by an electron gun initially firing a beam of electrons towards the sample. This beam is then focused by a number of condenser lenses usually in series. The beam then passes through the objective lens, with a series of deflection coils used to direct the focused beam of electrons and effectively scan the sample. The electrons interact with the sample and then reflect into a number of detectors such as a backscatter electron detector, and x-ray detector, or a number of secondary electron detectors. An illustration of such a setup can be seen in Fig. 14. The entire system is kept under vacuum. The overall magnification limit is approximately 500 000 times.

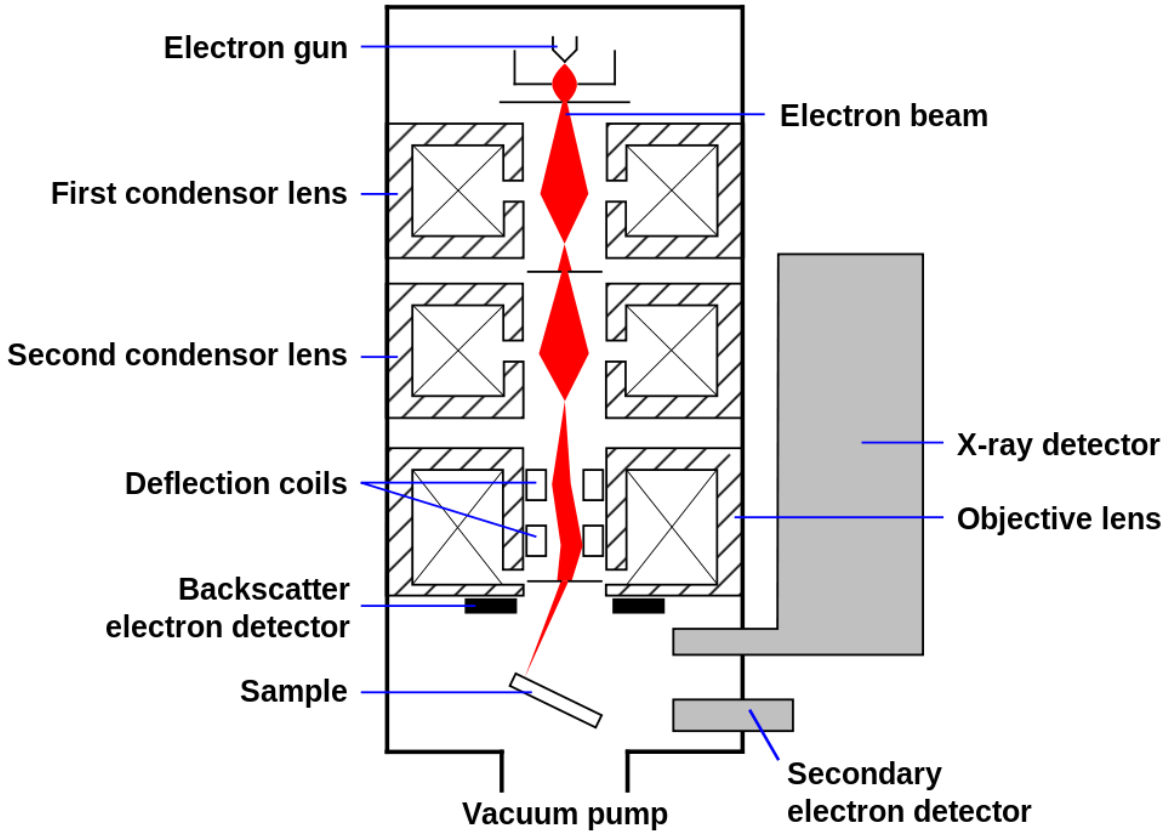

Figure 14: Basic Scanning Electron Microscope Schematic, usage licensed by creative commons attribution share alike 3.0 unported.

Samples used are typically conductive and grounded. This prevents the build up of electrostatic charge which can interfere with detectors. The three main types of detectors are inherently design to pick up on the three main types of signals produced by the electrons interacting. Backscatter electrons are those electrons which are reflected off the sample by elastic scattering. This type of signal and detector are often used to determine the composition of the materials, since the signal produced is strongly influenced by the size of the nucleus of the atoms. In order to examine specimen topography, a secondary electron detector is used. This detector interprets signals from electron interactions near the surface of the specimen, where the focused electron

beam is in contact with the sample. Similarly to backscatter electron detectors, an x-ray detector is used to determine atomic composition. In this work SEM is used to characterize the morphology of cobalt oxide bifunctional catalysts.

2.2 X-ray diffraction

X-ray diffraction is a form of x-ray crystallography where in the crystalline structure of a substances cause x-rays to diffract in unique directions. The intensity and angle of these reflected x-rays reveals information about the three dimensional structure of a substance. In order to provide information on a three dimensional structure, a series of two dimensional scans must be taken and integrated together. This is done through the use of a specific mount method wherein the sample may be mounted on a goniometre and rotated, or wherein the sample is fixed and the incident angle of the x-ray bombardment is altered. This analysis can be done through the use of various mathematical models, more specifically Fourier transforms.

One of the main principles of x-ray diffraction is Bragg's law, which addresses the determination of the angle of reflection or scattering from a crystal lattice. Brags law was first founded by William Lawrence Bragg in 1912. Bragg had discovered that at specific angles, x-ray diffraction peaks showed strong intensities, which could be used to identify specific crystal structures. X-rays where observed to effectively query inter-atomic spaces, due to the amplitude of the x-rays being similar in size to the distances between the atoms in most crystalline structures. Braggs law was derived based on the ideology that a crystal surface could be imaged as two parallel lines of atoms separated by distance D. This distance being the space between the surface atom and the one directly behind it. When an incident beam of x-rays is directed towards the crystal surface,

some of the rays will interact with the surface atom, while some will miss the surface atoms, and pass through to impact the atoms behind it. When the scattered rays from these interactions reacted constructively, a different magnitude of x-ray is formed wherein the change in magnitude is proportional to the distance between the surface atoms and those behind them. This causes an increase in intensity at specific incident angles, a seen in Fig. 15.

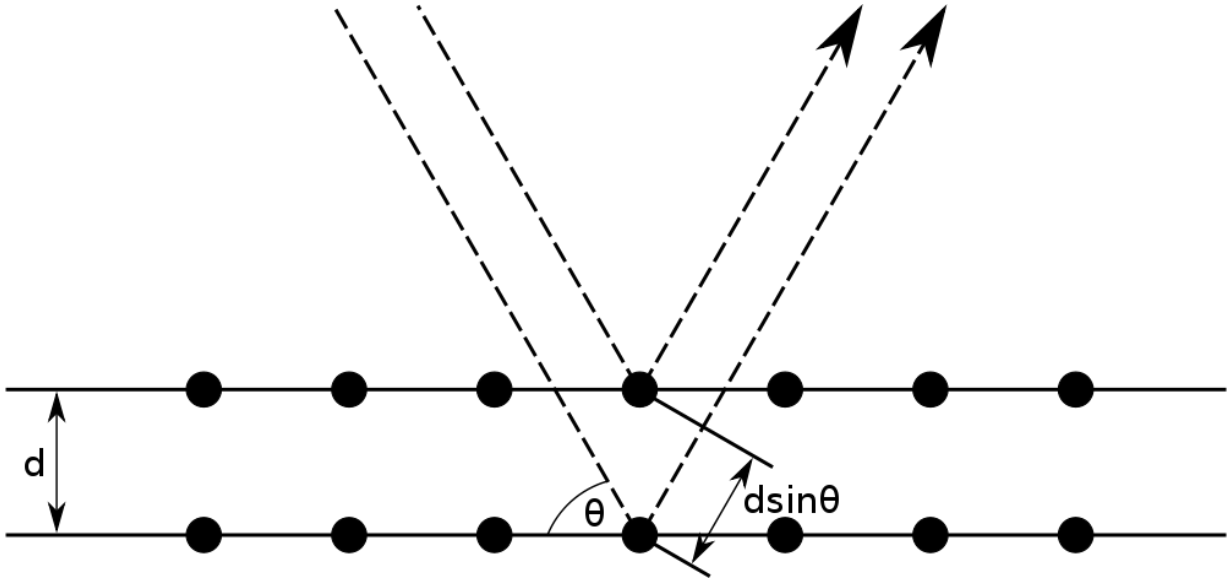

Figure 15: Illustration of Bragg diffraction observed in and atomic lattice

This constructive interference is shown to occur only when the observed phase shift is a multiple of 2π. Bragg's law can be expressed as:

$$n\lambda = 2d(sin\theta) \qquad (1)$$

Where n is an integer, λ is the incident wavelength, d is the distance between planes in the crystal lattice, an θ is the angle between the scattering plane and the incident x-rays. In this work XRD is

used to determine and compare crystal structure of cobalt oxide nanosheets and nanoparticles. XRD is also used to confirm proper spinel type cobalt oxide synthesis.

2.3 Energy Dispersive X-ray Spectroscopy

Energy Dispersive X-ray spectroscopy is an elemental analysis method which focuses on identifying elemental x-ray signatures. The process of producing recognizable and unique energy signatures from specific elements begins with the targeting of an external stimulation. This stimulation can be a concentrated beam of electrons, protons, or x-rays. Upon incident interaction of this stimuli with the inner electrons of an element, said inner electron may be forced from the system. An electron from a higher energy orbital is then required to fill the void. This difference in energy between these two electrons states is released in the form of radiation energy, which can be detected by an energy dispersive spectrometer. An illustration of this process can be seen in Fig. 16. In this work EDAX is used to analyze the composition of porous anodes and confirm removal of ammonium chloride within the structure.

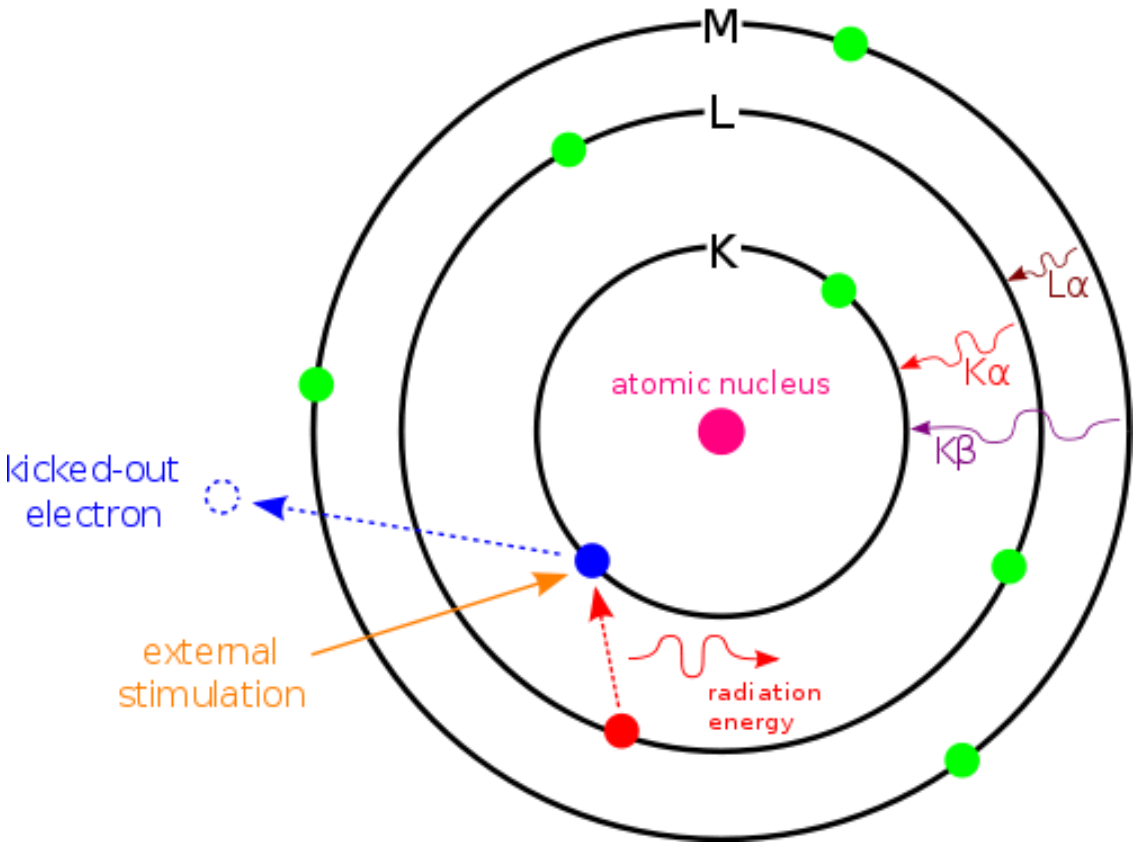

Figure 16: Illustration of the formation of radiation energy by external stimulus for EDX, usage licensed by creative commons attribution share alike 3.0 unported.

Due to the dual requirements of electrons beam sources by SEM and EDX, often a single source may be utilized for both types of analysis in a combined system.

2.4 Half Cell Electrochemical Testing

It is often inefficient to undergo full cell testing for multiple catalysts, as full cell testing for durability can take upwards of two weeks depending on the durability of the catalyst. For this reason it is helpful to screen potential catalysts for full cell testing with half cell electrochemical testing. For the purposes of this study half cell testing was completed using rotating ring disk electrode voltammetry (RRDE). The basic setup for RRDE consists of a main reaction vessel,

which in this case is a 500mL three neck flask. The most common electrolyte used for half cell reactions of this nature is 0.1M potassium hydroxide, and that is the electrolyte in which the reactor flask was filled. The setup involves three electrodes, a working, reference, and counter electrode, hence the three necks of the flask. The working electrode in mounted onto a rotating shaft controlled by a low power motor. The working electrode consists of a glassy carbon electrode surrounded by a platinum ring electrode. The carbon electrode as an outer diameter of 5mm and the platinum ring electrode has an inner and out diameter of 6.5mm and 7.5mm respectively. The reference electrode consisted of a double junction silver/silver chloride (Ag/AgCl) electrode, and counter electrode used was a platinum wire. The electrode were connected to a bipotentiostat (Pine instruments, model number AFCBP1) for all RRDE analysis. A schematic is visible in Fig. 17.

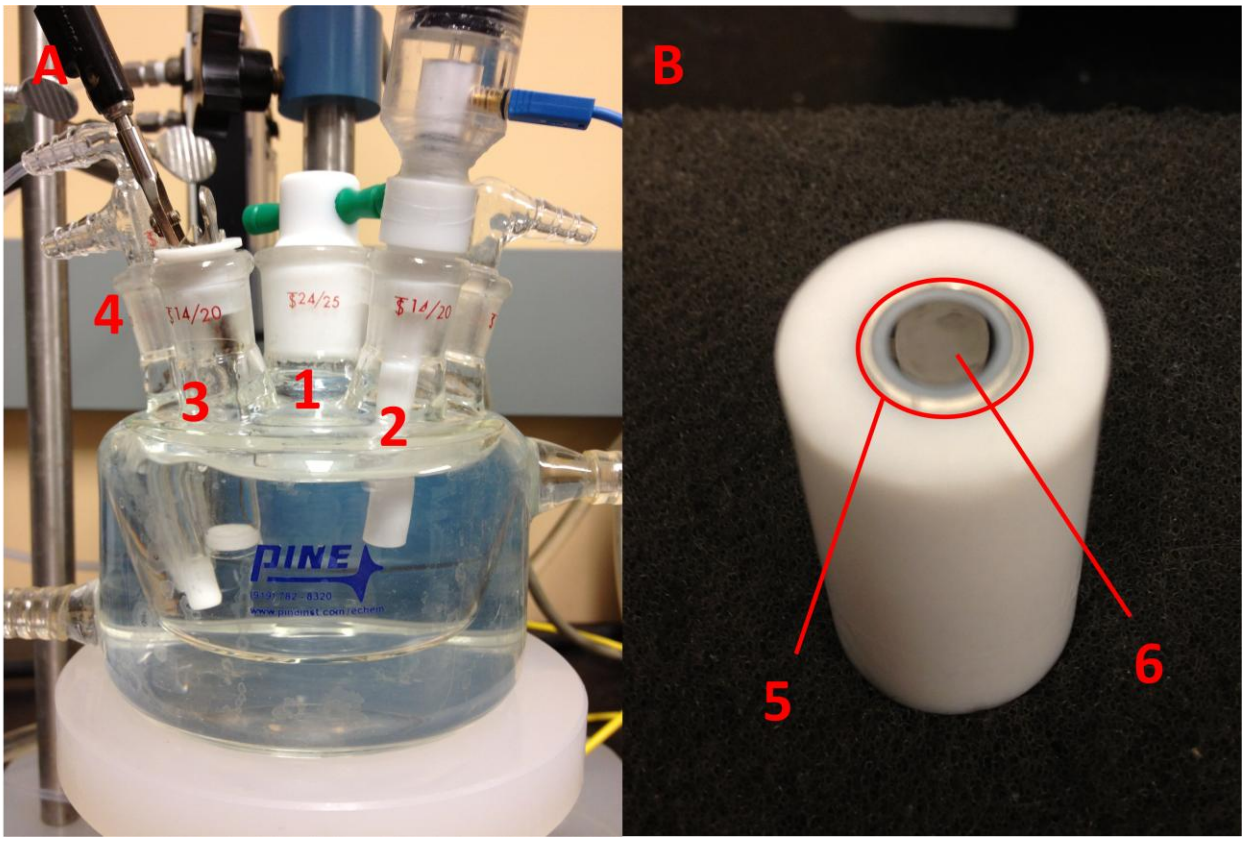

Figure 17: A) Schematic of RRDE setup with 5 neck flask, B) Working electrode showing glassy carbon and platinum ring

Table 2: List of half cell potential apparatus and components

Identification	Item Description
1	Working Electrode
2	Ag/AgCl reference electrode
3	Platinum wire/counter electrode
4	Gas bubble/gas input
5	Platinum (99.99%) ring electrode
6	Glassy carbon electrode.

A catalyst ink is prepared, similar to that of full cell testing. The ink was prepared by first mixing 2mg of catalyst into 1 mL of isopropyl alcohol. This mixture was then ultrasonicated for approximately 30 minutes before 67µL of 5wt% Nafion solution was added. This nafion solution

was created by diluting a stock 15wt% solution (Liquion Solution LQ-1115 1100EW 15 wt.%). The solution was further ultrasonicated for another 30 minutes or until well dispersed. Of this ink, 10μL is deposited onto the glassy carbon electrode and dried. There are several advantages to the use of RRDE, one of those being the ease of control of reactants to the working electrode. In the case of analyzing ORR kinetics, oxygen is bubbled into the electrolyte solution to attempt to saturate the solution with oxygen. Mass transport kinetics are controlled by the speed at which the working electrode is rotated. This laminar flow of electrolyte caused by rotation controls the flow of oxygen to the surface of the working electrode.

There are two main types of analysis completed by RRDE using the bipotentiostat, those being cyclic voltammetry and linear scan voltammetry. Cyclic voltammetery involves sweeping of the working electrode potential between two set potentials, where as linear scan voltammetry only sweeps in one direction. For cyclic voltammetry testing, the capacitance can be calculated based on the integrated area under the CV curve, as seen in Fig. 18.

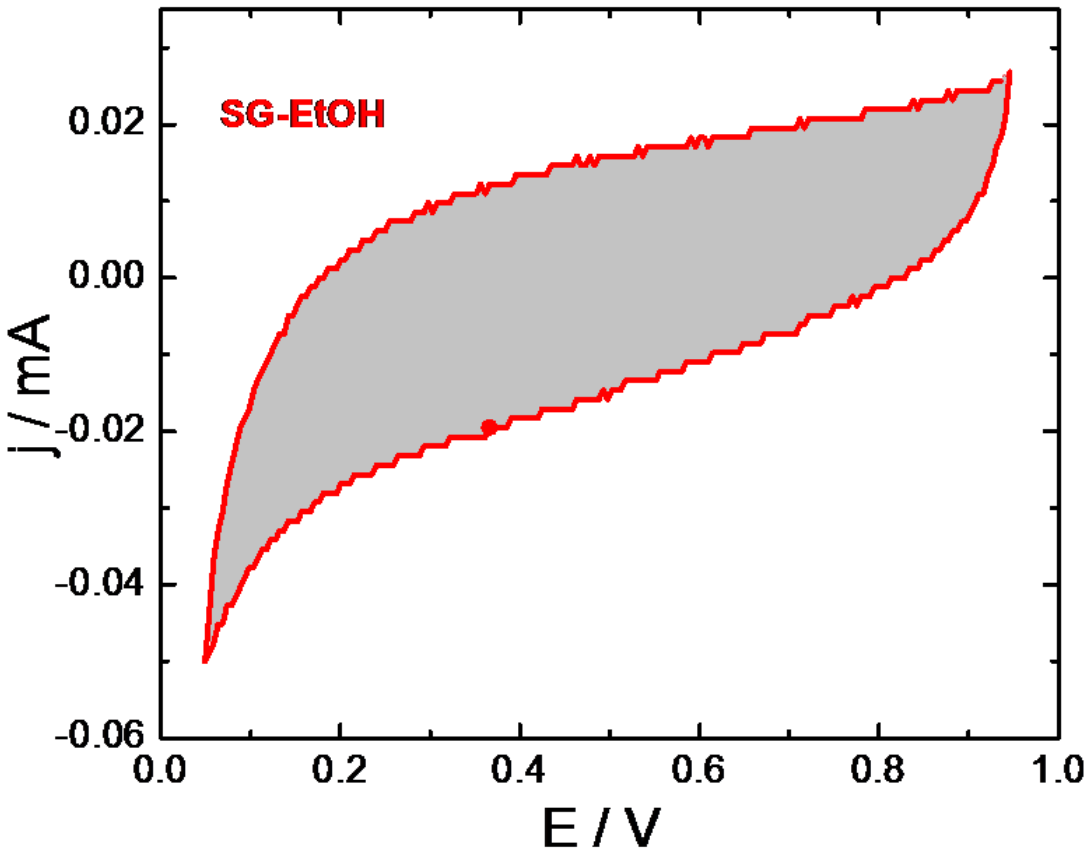

Figure 18: Cyclic voltammagram for sulfur doped graphene, area under CV curve highlighted grey.

Linear scan voltammetry utilizes a sweep in potential of the working electrode with respect to the reference electrode. This sweep is generally from that of high potential to a lower potential. The sweeping rate may be varied, however in this thesis, all sweeping rates were kept constant at 10mV/second. The background current or capacitive current of a catalyst may be tested by conducting linear sweep voltammetry on a sample in the absence of oxygen. For this the electrolyte is purged with nitrogen, removing all oxygen from solution. When conducting linear sweep to determine catalytic activity, the system is purged with oxygen, thus allowing the ORR reactions to proceed with controlled mass transport from the rotating electrode. In both cases the

system is purged with either oxygen or nitrogen for 30 minutes, until which the electrolyte is considered saturated.

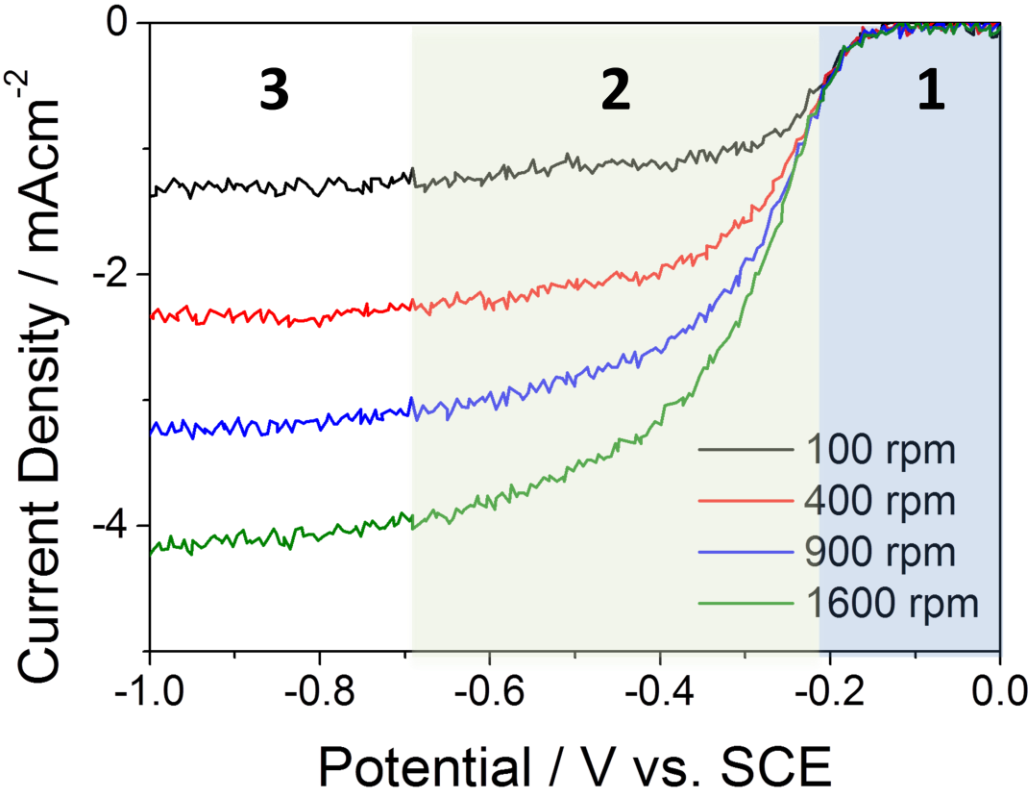

Figure 19: Typical polarization curve from linear sweep voltammetry, with three regions identified (cobalt oxide and graphene catalyst)

There are three regions of a typical polarization curve, each corresponding various limitation on the reaction. The first region is based on kinetic limitation wherein reaction kinetics are the limiting factor in the reaction rate. In this case rotation speed and mass transfer have no real influence on the reaction rate, as seen by Fig. 19 where all four rotation speeds yield the same current density and potential. The second region is a mixed control region in which both reaction kinetics and mass transport have influence on the rate of reaction. A deviation in the reaction

rates can be observed in different rotation speeds during this mixed region, indicating the limitation of mass transport to the working electrode. The third region is one in which reaction rate is almost entirely limited by mass transport. The rotation speed is clearly seen has having almost sole influence on current density observed. As the reaction kinetics are increased a higher rate than the rate of delivery of oxygen to the working electrode, then the reaction becomes mass transfer limited. A good catalyst will have a very short initial kinetically limited region, and longer mass transfer limited region, indicating that the reaction kinetics of the catalyst are relatively fast.

The electrochemical kintetics of the reaction in half cell testing can be further understood through the Koutecky Levich equation. The current density observed can be analyzed by the following equation.

$$\frac{1}{i} = \frac{1}{i_k} + \frac{1}{i_d} \qquad (2)$$

Where i_k is the kinetically limited current density, i_d is the diffusion limited current density, and the overall current is defined by i. i_d is dependent on the rotation speed of the working electrode (ω) and be defined by the following equation.

$$i_d = 0.62nF[O_2]{D_{O2}}^{2/3}\nu^{-1/6}\omega^{1/2} \qquad (3)$$

Where F is faradays constant, n is the number of electrons transferred via the reaction, $[O_2]$ is the concentration is solution, assumed to be the saturated concentration of O_2 in the electrolyte, D_{O2} is the diffusion coefficient for oxygen in the electrolyte which is also constant, and v is the inherent viscosity of the caustic electrolyte. The diffusion coefficient for oxyen in the electrolyte is $1.9x10^{-5}$ cm^2s^{-1}, the concentration of oxygen in saturated solution is $1.1x10^{-6}molcm^{-3}$, and the

kinematic viscosity of the electrolyte solution is 0.01 cm^2s^{-1}. The only variable in the above equation is ω, which allows the above equation to more simplified as,

$$\frac{1}{i} = \frac{1}{i_k} + \frac{1}{B\omega^{1/2}} \qquad (4)$$

Where,

$$B = 0.62nF[O_2]{D_{O2}}^{2/3}v^{-1/6} \qquad (5)$$

A Koutecky Levich plot can be made by plotting 1/I versus ω for the various sweep potentials completed in the linear scan experiment. The y intercept of this plot represents the kinetically limited current density. The lope of the plot is used to determine the number of electrons transferred in the reaction. This goes with following the two electron pathways in which the oxygen reduction reaction can properly occur. The four electron transfer reaction is most efficient; however the catalyst will not use this pathway 100% of the time. Therefore the number of transferred electrons will be an average number, the closer this is to four, the more often that ORR is occurring through the four electron pathways, and the more efficient the catalyst.

Cyclic voltammetry is used in this work to preemptively analyze cobalt oxide nanosheets viability and durability as a bifunctional catalyst.

2.5 Full Cell Testing

The full cell testing completed in our laboratory utilizes a multichannel potentiostat which can complete both galvanodynamic and galvanostatic testing. The full cell used for testing is made from four pieces of clear acrylic which are used as the base structural components of the cell. These acrylic plates are separated by several rubber gaskets which ensure no electrolyte leakage.

The two middle acrylic plates act as the electrolyte reservoir, with a polypropylene separator or PTFE membrane between them. These plates have 4mm diameter holes drilled in upper portion of the plate leading towards the center, which allows for the addition of electrolyte to the cell as well as allows gas to escape the cell. This is important due to the hydrogen and oxygen evolution which occurs during the charge and discharge of the cell. The most basic cell consists of a solid zinc plate anode backed by a stainless steel mesh current collector, which protrudes from the top of the cell were the devices can be connected to the potentiostat. The most basic cathode design consists of carbon fiber gas diffusion layer (GDL) with a layer of amorphous carbon on which the bifunctional catalyst may be loaded. The cathode is similarly backed by a stainless steel mesh current collector which protrudes from the top of the cell. The acrylic plate located on the cathode side of the cell as an opening which allows air flow through the GDL towards the amorphous carbon layer and catalyst. The GDL is also treated to be hydrophobic, and prohibits electrolyte leakage through this opening. The entire cell is held together by four bolts securing all four corners of the acrylic plates. A full schematic is seen by Fig. 20.

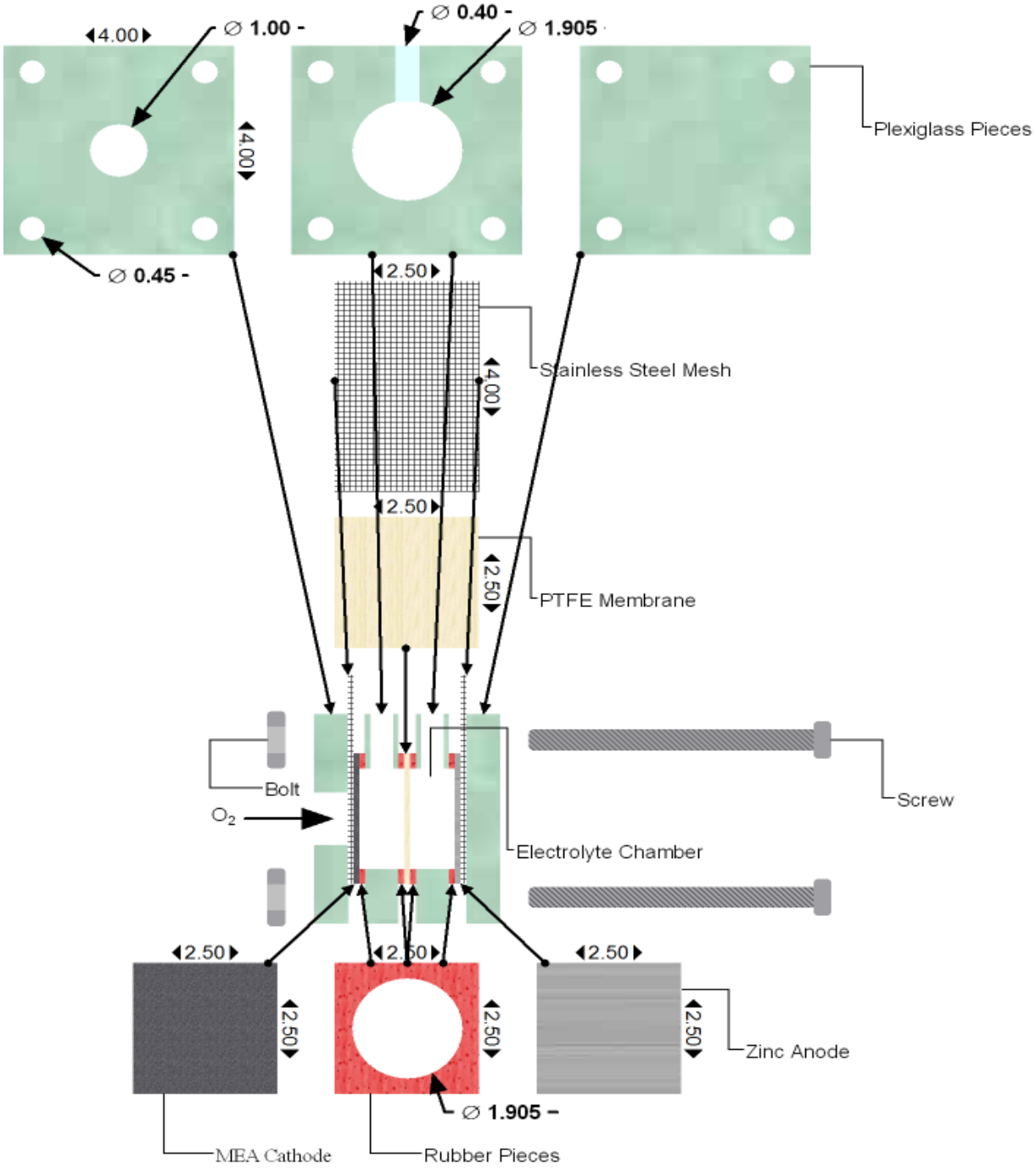

Figure 20: Basic acrylic zinc air battery schematic [5]

3.0 Porous Zinc Electrodes Via Sublimation

3.1 Introduction and Purpose

Several methods have been employed to create non solid anodes for use in zinc air cells, wherein the higher surface area of these non solid anodes can greatly aid performance. Powder anodes can be made by gelling zinc powder. The porosity or void space is controlled by gelling, however the extent to which this can be done is limited based on the powder size. Additionally, the anode is not a single piece, and can have conductivity issues. Fibrous anodes can be made by spinning off molten zinc into fibers and compressing those fibers. These can be made into various shapes, however dendrite formation is not addressed, and durability is only moderate. Additionally, the process requires dealing with molten zinc, which requires high temperatures. Another disadvantage is that the void shape is limited to the elongated formations between the fibers. Since the fibers are often large, pore sizes in the nano range are near impossible. Therefore surface area is considerably lower than the atomized zinc powders. The new method involves a simple two step procedure for the synthesis of porous anodes in a facile and economical way. One benefit of the procedure is the green chemistry aspect of synthesis wherein all chemicals used are environmentally safe, and recoverable as well as reusable. This not only reduces the environmental impact of production but additionally increases its economic viability. In the first step of the process, a mixture of the base anode material, that being zinc or zinc alloy, and the filler sublimation/decomposition compound is pressed at high pressure to desired form. This mixture can be pressed around a support or current collecting structure, or be free standing. Once pressed, the formed anode is heated to approximately 350ºC for a period of time dependent on the filler compound, to the point where the sublimation/decomposition filler compound is

allowed to dissipate from the sample, and the zinc or zinc alloy structure becomes annealed. If the filler compound sublimes/decomposes, such as with aluminum and ammonium chloride, the compound may be recovered later in processing. This reduces the overall cost of the process, wherein all material is recoverable, and all treatment is done in a single step.

3.2 Experimental Procedure for Producing Porous Metal Foams Via Filler Sublimation

3.2.1 Ideology behind Sublimation Process

The porous anodes fabricated in this study serve to show proof of concept in which porous metal plates of varying porosity and pore sizes can be synthesized by a single heating step. This process takes advantage of the low annealing temperature for zinc, and uses this to simultaneously improve structural integrity of the porous plate while forming the pore structure. Some porous plates and anodes are formed via erosion of a filler compound in caustic or acidic environments, wherein the filler compound is initially mixed with a zinc powder and either made into a paste or pellet. This pellet is then submersed in either caustic or acidic environments for extended periods of time, often requiring more than a single day to complete the erosion of the filler compound. The porous pellets produced by this process are found to be structurally unstable, due to the fact that the entirety of the structural stability of the pellet is based solely on the high pressure compression of the zinc and filler powder mixture. The sublimation process varies from this ideology in the sense that instead of using caustic or acid environment to erode the filler compound, the compound may be sublimated away similar to a freeze drying process, leaving the pellet with very well defined pores. This process is completed by initially mixing zinc powder with a filler compound which sublimes at around 350°C. The mixture is pressed into a pellet form, and then heated to the appropriate temperature at which sublimation occurs.

The annealing temperature of zinc can be as low as 300°C, and therefore by heating to temperature greater than this the zinc structure is annealed. This greatly improves the structural stability of the porous anode. The overall process is illustrated by Fig. 21.

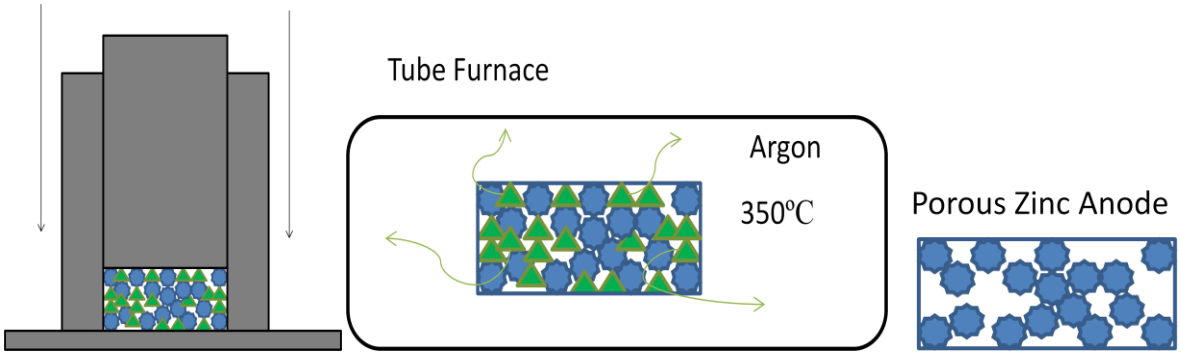

Figure 21: Schematic of an example of the fabrication process, using zinc and ammonium chloride

The temperature required to sublimate or decompose the filler could be less than the annealing temperature of the base material, however, a second heat treatment step to anneal the anode should be performed. The structured porous anode has good conductivity due to the interconnected nature of the porous structure. Additionally the surface area, porosity, and overall structure can be altered due to varying process parameters, such as the particle size of the zinc or filler compound as well as annealing time and temperature. Additionally, the issue of dendrite formation can be partially addressed by the pressing of the powder mixture around copper foam, or various other support structures. Similarly, dendrite formation can be further addressed through the alloying of the zinc powder used. For example, the zinc could be alloyed with indium and nickel in varying ratios which are shown to drastically reduce dendrite formation. Lastly, the coating or addition of various polymers to the anode can be used to reduce dendrite formation further and improve performance and durability.

3.2.2 Specific Experimental Methods

The porous anode was prepared using a base anode material of atomized zinc powder. The filler compound selected for use was ammonium chloride. No support was used, and the anode was free standing. The anode was pressed using a hydraulic press, to a pressure at which the anode remained a single unbroken piece (5 atm), as seen in Fig. 22. The anode was then placed in a tube furnace inside of a quartz tube. The anode was heated to 350ºC with a ramp rate of 10ºC per minute, under an argon atmosphere in order to avoid unnecessary oxidation of the zinc. The sample was similarly cooled at a rate of 10 ºC per minute under argon, and then removed from the furnace and washed with water to remove any zinc chloride that might have formed due to reaction with HCl released by the ammonium chloride. The sample was further dried in air at 60ºC for 2 hours.

Prior to full cell testing, the air electrode was prepared by spray coating of a catalyst ink onto a carbon based gas diffusion layer. The ink was prepared by first mixing 10mg of catalyst into 1 mL of isopropyl alcohol. This mixture was then ultrasonicated for approximately 30 minutes before 67µL of 5wt% Nafion^{TM} solution was added. This Nafion^{TM} solution was created by diluting a stock 15wt% solution (Liquion Solution LQ-1115 1100EW 15 wt.%). The solution was further ultrasonicated for another 30 minutes before being spray coated onto the carbon gas diffusion layer (Ion Power Inc., SGL Carbon 10 BB, 2.5 cm×2.5 cm). The ink was sprayed to achieve a loading of 1.5mgcm^{-1}. The GDL was then dried in an oven for 1 hour at 60°C. The cell was fabricated using a polypropylene separator (Cellgaurd 5550). The cell was fabricated using a stainless steel current collector fastened behind the porous zinc anode and the GDL loaded with

catalyst. The cell was assembled following the previous design specifications with approximately 2mL of 6M KOH (Sigma Aldrich). Full cell cycling was completed completed using the multichannel potentiostat (Princeton Applied Research, VersaSTAT MC) using recurrent galvanic pulses of 50mA. Each cycle consisted of 300 second discharge step followed by a 300 second charging step. Galvanodynamic testing was completed by scaling the current from 0 to 300mA at a rate of 5mA per second.

3.5 Results and Discussion

The porous anodes were effectively synthesized and viewed under a light microscope at 60x magnification as seen in Fig. 22,23.

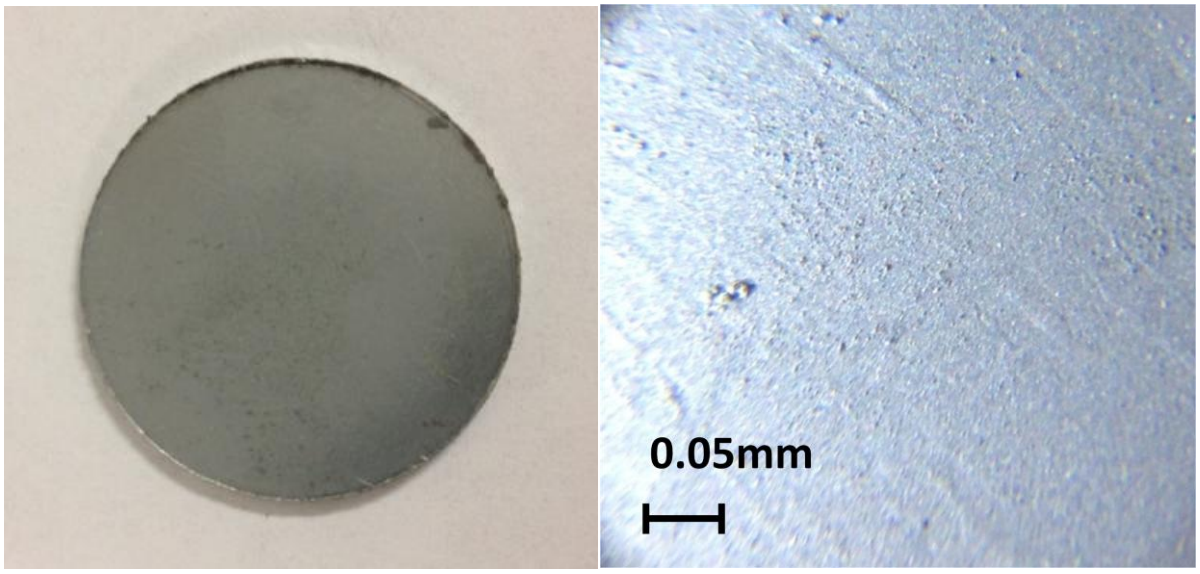

Figure 22: Pressed disk consisting of atomized zinc powder and ammonium chloride, 60x magnification of the pressed disk.

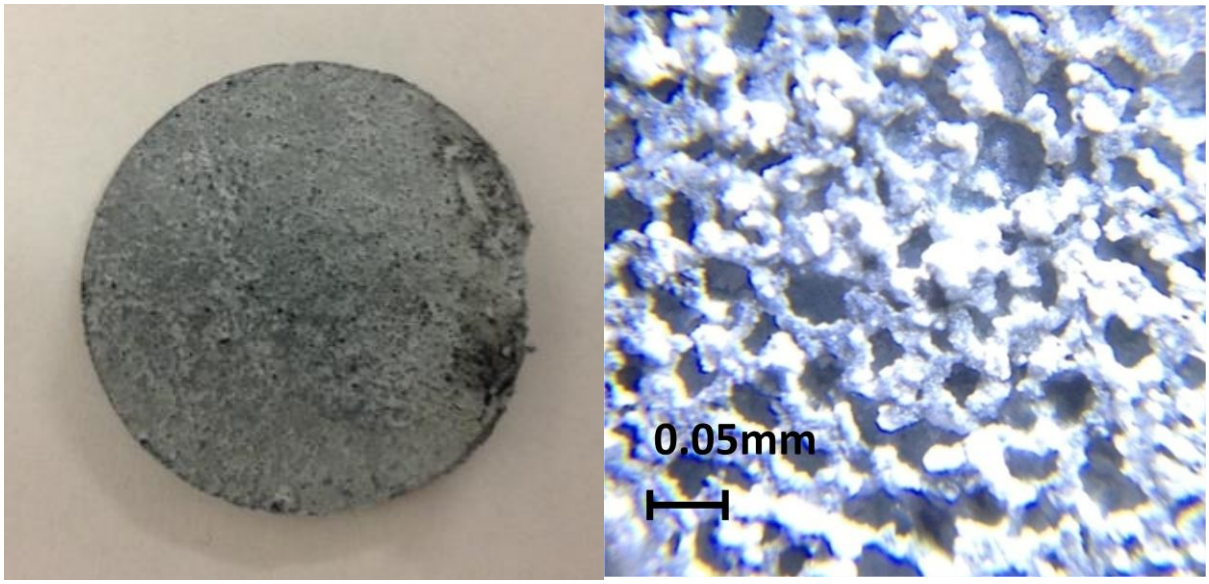

Figure 23: Pressed disk after heat treatment, ammonium chloride should be removed, 60x magnification of heat treated pressed disk.

It can be clearly seen from Fig. 22 and 23 that the anode becomes significantly more porous after the heat treatment process, indicating that the process is successful in creating porous anodes. It can be noted from Fig. 23 that the pores created in this anode are in fact quite large, as compared to the atomized zinc particles visible in Fig. 22. This large pore size is due to particle size of the filler compound which was used. By altering the filler particle size you can in theory alter the pore size to any desired formation. However, if the heating cycle ramps overly quickly or the treatment temperature is too high, bubbles will be formed as the filler material sublimates. This gas expansion causes larger pore sizes than that of the filler compound.

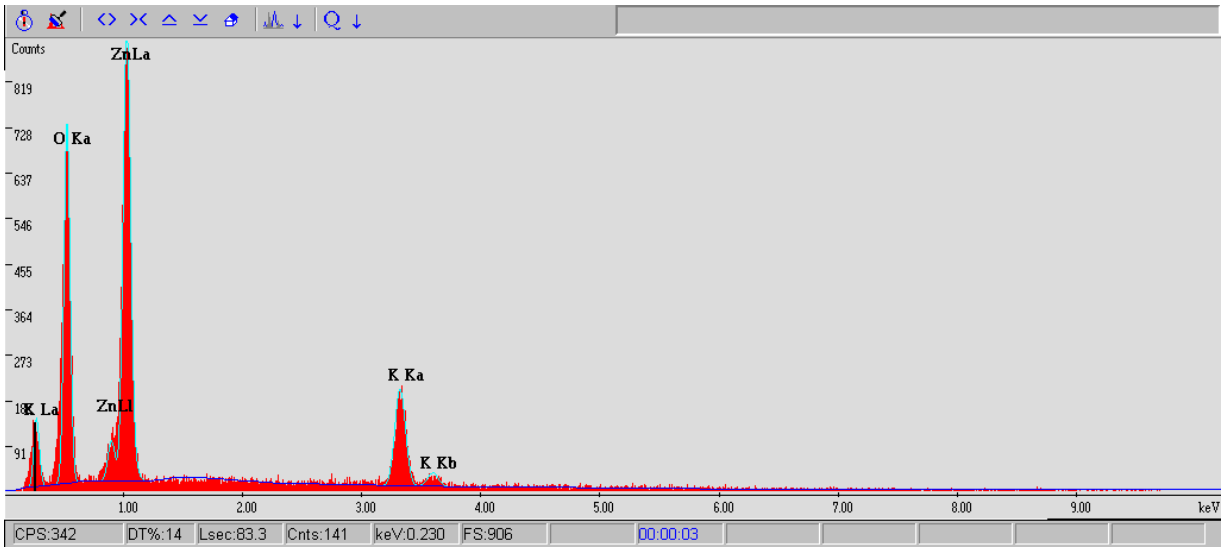

Figure 24: EDAX showing plate anode composition after full cell cycling in 6M KOH.

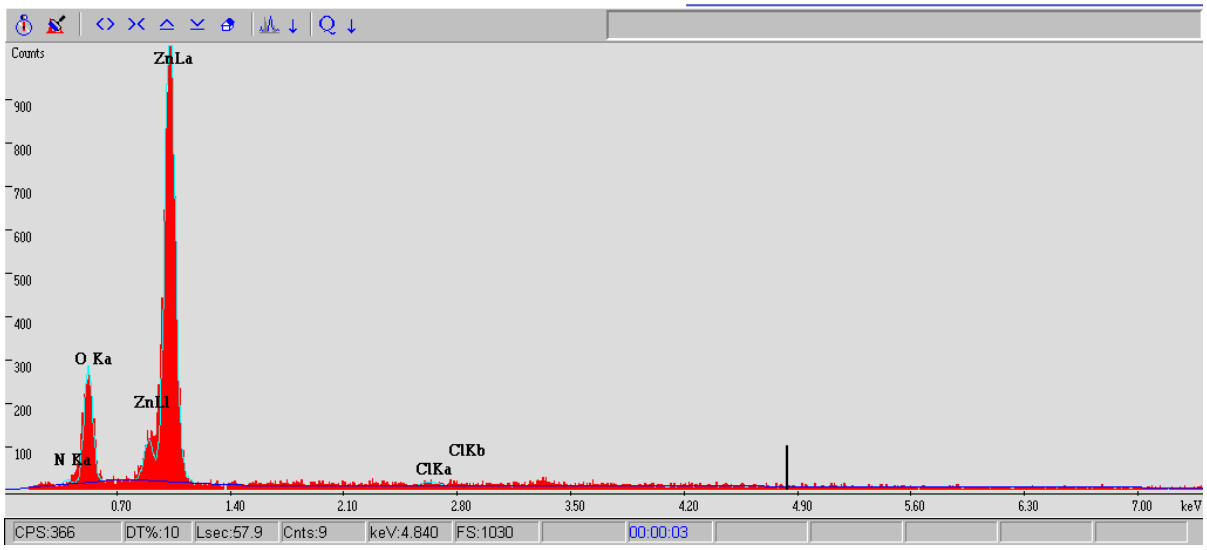

Figure 25: EDX showing porous anode composition after full cell cycling in 6M KOH

Table 3: Comparison of EDX results for both the plate and porous anode after full cell cycling in 6M KOH

Element	Plate Anode (Wt%)	Porous Anode (Wt%)
O	28.36	14.06
Zn	51.97	83.64
K	19.67	-
Cl	-	0.93
N	-	1.36

It can clearly be seen from Table 3 and Fig. 25 that there is some nitrogen and chlorine present in the porous anode even after full cycling. This is due to trapped ammonium chloride that was unable to sublimate and leave the pellet properly during the heating cycle. This can easily be fixed by adjusting the ratio of atomized zinc powder to filler compound in order to create a more porous network, in which ammonium chloride could not be trapped. This would apply to all types of filler compounds used. Similarly so, by using larger particles of filler compound you could also create a more porous network, solving the issue of trapped filler compound.

A significant improvement in charge and discharge performance was clearly visible in Fig. 26. The porous anode was able to hold a higher discharge potential at higher currents than the standard plate anode. This is due to the increased surface area which is exposed to electrolyte accompanying the porous anode. Similarly, the porous anode was able to charge at a much lower potential than the plate anode. This is again due to the increase anode surface area. This lower charging voltage coincides with large improvements in efficiency. At lower potentials, less hydrogen evolution occurs in the cell, resulting in a much higher charging efficiency.

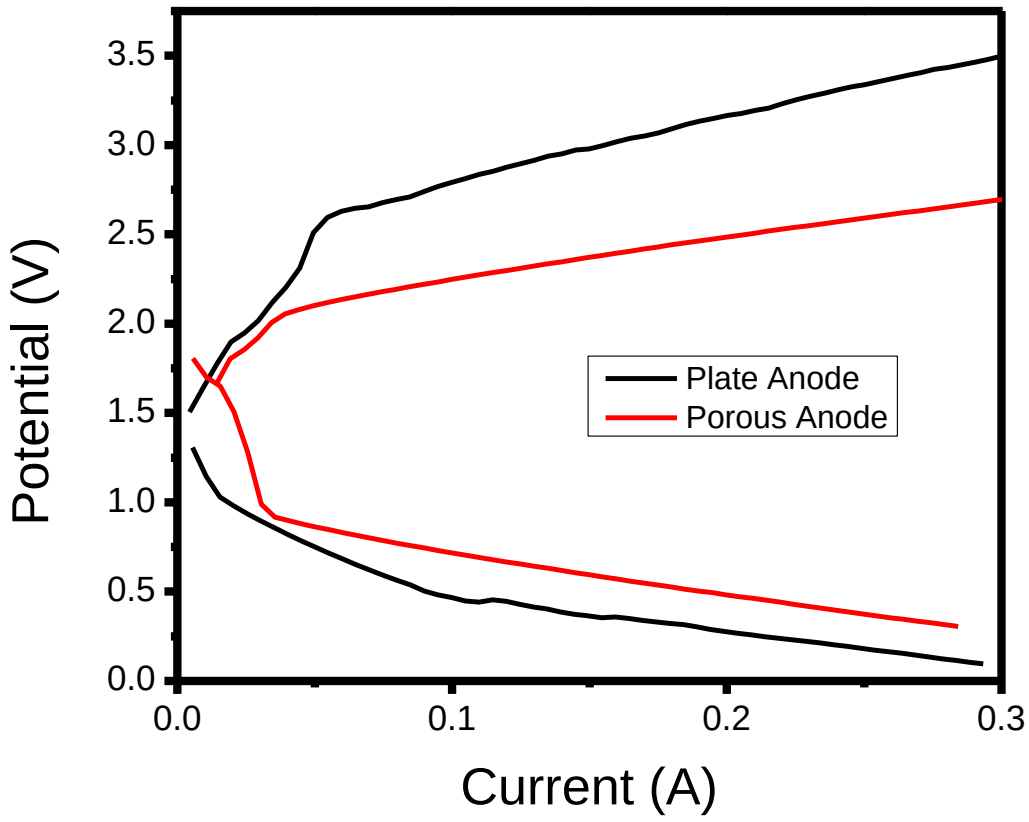

Figure 26: Charge and discharge comparison of porous zinc anode to zinc plate anode.

Table 4: Comparison of the charge and discharge performance of both the plate and new porous anode at currents of 100mA, 200mA, and 300mA

Current	100mA	200mA	300mA
Average Discharge potential (V) Plate	0.582085	0.332	0.106
Average Discharge Potential (V) Porous	0.7003	0.47535	0.306
Average Charge Potential (V) Plate	2.7565	3.155	3.495
Average Charge Potential (V) Porous	2.2455	2.4655	2.6732

Table 4 clearly shows that at all currents up to 300mA, the porous anode significantly out performs the plate anode. A difference in discharge potential of approximate 0.12V at 100mA, 1.4V at 200mA, and 0.2 volts at 300mA can be seen. There is a noticeable trend indicating that at higher currents, the difference in performance increases. This shows promise for porous anodes to be significantly more appropriate than plate anodes in high current systems, such as those required for electric vehicles and hybrid electric vehicles. A difference in charging potentials can also be observed. The difference is approximately 0.51V at 100mA, 0.69V at 200mA, and 0.82V at 300mA. A similar trend is observed for charging potential where in the difference in potentials between the plate and porous anode increase with and increasing current.

3.5 Conclusions

The sublimation process was successful in creating porous zinc anodes for zinc air batteries. Although some filler compound can become trapped in the porous network, this problem can be easily fixed by adjusting the ratio of filler compound to atomized zinc powder, or by using varying sizes of filler compound. Both of these solutions are aimed at creating a more open porous network which will not trap the filler compound during the heat treatment process. The porous anodes showed significantly higher performance than standard plate anodes in full cell galvanodynamic testing. This higher performance was further amplified at higher currents, indicating promise for these anodes in high current systems.

4.0 Advanced Carbon Limited Gas Diffusion Electrode

4.1 Introduction and Purpose

Currently, the majority of metal air battery fabrication use a Gas Diffusion Electrode in academia and research, wherein this is the common choice for cathode design. Most often, the catalyst being studied is adhered via polymers binders or other binding methods to a type of carbon gas diffusion layer (GDL). This gas diffusion layer has three main aspects of design which allow it function well in the situations in which it is currently used. The GDL consists of a carbon fiber sheet structural base, which is both porous and permeable to air and aqueous electrolyte. This structural base has a layer of amorphous carbon on one face, and a layer of polytetraflouroethylene (PTFE) coating on the other face. The amourphous carbon layer is where the active catalyst is deposited onto the gas diffusion layer. This high surface area and conductive material allows for the active bifunctional catalyst to preform both the oxygen evolution and oxygen reduction reactions necessary for metal air battery function. A current collector is placed behind, but in contact with the GDL to allow for current flow from the catalyst through the circuit and vice versa. The PTFE coating prevents the aqueous electrolyte (usually caustic) from leaking through the GDL and out of the cell. Overall, the cathode design of these rechargeable metal air battery cells consists of the bifunctional catalyst loaded onto the GDL, which is backed by a current collector. There are many current issues with durability of metal air cells, which are often thought to only be viable for a few hundred cycles of use. One of these issues is thought to be carbon corrosion, wherein the amorphous carbon on which the catalyst is loaded is thought to degrade and corrode due to the oxygen presence and caustic nature of the electrolyte. This corrosion causes loss of active catalyst material as when the carbon

in which the catalyst is loaded on corrodes, there is nothing adhering said catalyst to the conductive GDL, and thus the reactions generate no current.

4.2 Experimental Procedure and Electrode Design

4.2.1 Electrode Design

The design in its most basic form incorporates the use of non-carbon materials on which the catalyst is loaded. These caustic resistant, conductive materials also function as the current collector for the electrode. Various forms of GDL can then be incorporated onto the backside of the material to facilitate gas diffusion towards the active bifunctional catalyst material. One particular material of choice for use in this design is stainless steel in the form of a mesh or foam, however many other materials may be used such as titanium, titanium alloys, brass, nickel and nickel alloys, or other conductive, caustic resistant, non-carbon based materials. Specific types of stainless steel are extremely caustic resistant, non-carbon based and conductive, fulfilling all requirements of the design. The bifunctional catalyst can then be bound to the stainless steel mesh or foam via common binders such as Nafion^{TM}, or polyvinyl alcohol. This binding can be completed in many ways, however one simple method of binding the catalyst to the mesh involves spray or brush coating of a catalyst ink. This ink is formulated by ultrasonicating the catalyst in a solvent such as isopropyl alcohol, and subsequently adding the binder after some period of time. The completed ink is then further ultrasonicated for 30 minutes to improve dispersion. This ink can then be directly applied to the stainless steel mesh or foam via spraying from an aerosol sprayer or air brush. The stainless steel mesh or foam and loaded catalyst can then be dried to remove the solvent if necessary. This can be completed on many layers of mesh or foam, which are placed in series to further improve catalyst loading and surface area of the

electrode as seen by Fig. 27, 28. This catalyst loaded material, henceforth referred to as active layer, can then be backed by a gas diffusion layer. This diffusion layer can consist of carbon fiber either bound or pressed together to form a porous sheet, or other materials such as polymer fibers. The active layer can be pressed, bound, or freely placed against this carbon or polymer fiber sheet. Finally, a layer of PTFE is added to the back of the carbon or polymer fiber sheet to act as a hydrophobic layer, which is required to prevent liquid electrolyte from leaking out of the cell.

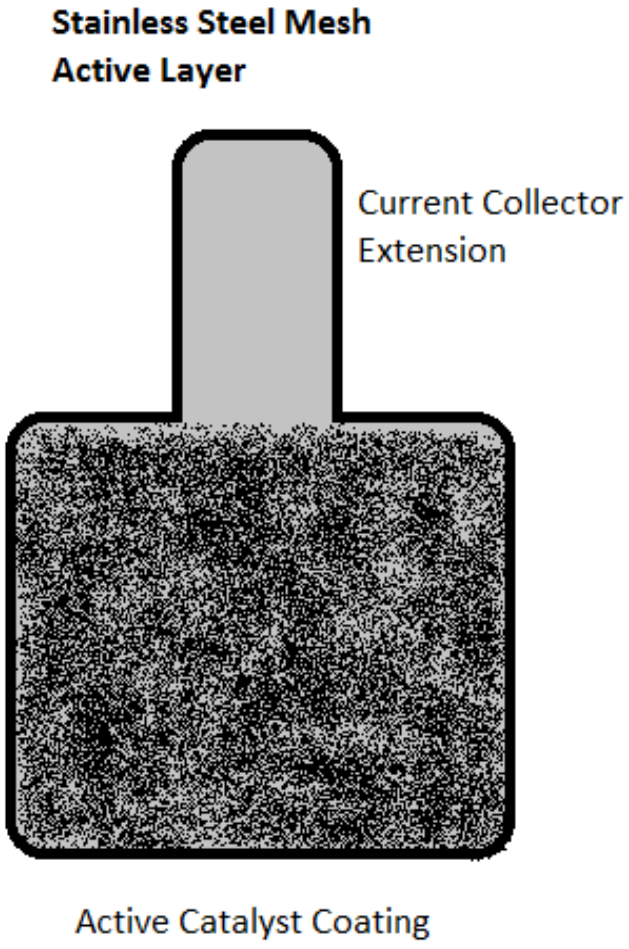

Figure 27: Stainless steel mesh active layer with spray on catalyst loading

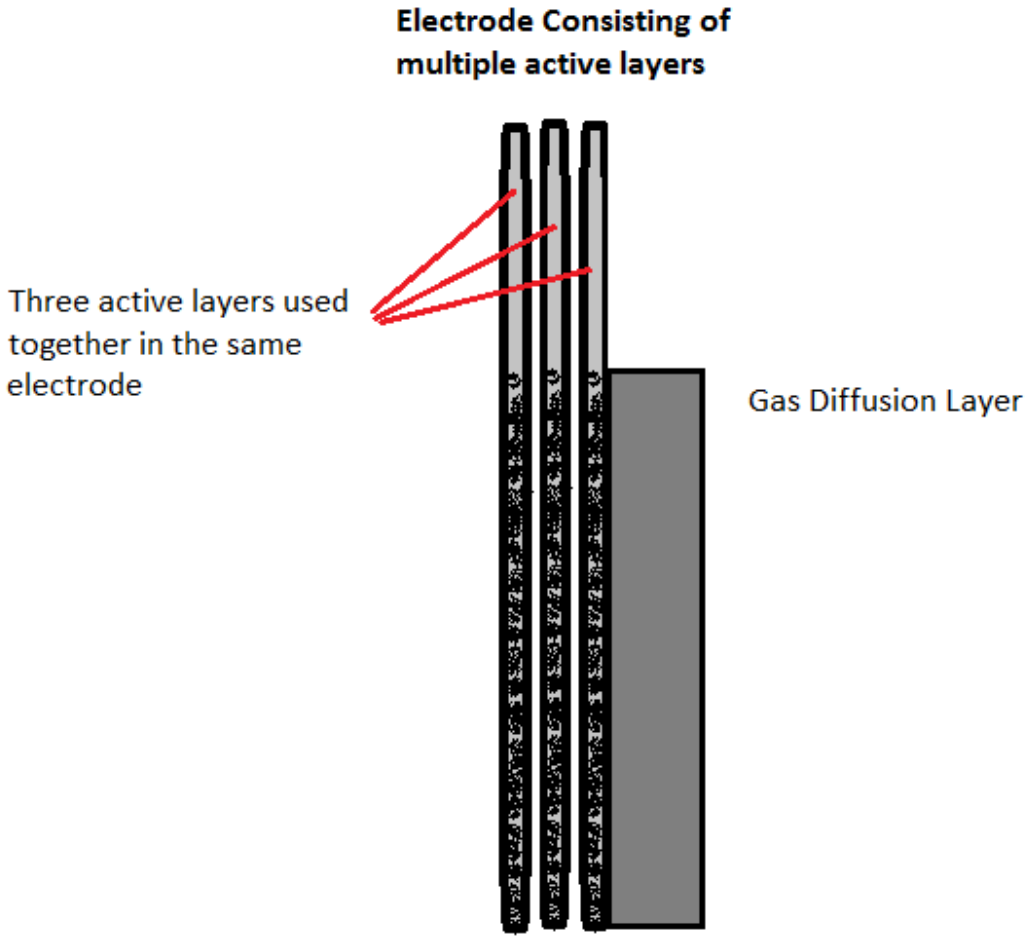

Figure 28: Electrode consisting of multiple active layers with spray on catalyst loading

4.2.2 Experimental design and specifics

Prior to full cell testing, the air electrode was prepared by brush coating of a catalyst ink onto a 6.25cm² square piece of stainless steel mesh. The ink was prepared by first mixing 10mg of catalyst into 1 mL of isopropyl alcohol. This mixture was then ultrasonicated for approximately

30 minutes before 67µL of 5wt% Nafion^{TM} solution was added. This Nafion^{TM} solution was created by diluting a stock 15wt% solution (Liquion Solution LQ-1115 1100EW 15 wt.%). The solution was further ultrasonicated for another 30 minutes before being spray coated onto the c air carbon gas diffusion layer (Ion Power Inc., SGL Carbon 10 BB, 2.5 cm×2.5 cm). The ink was sprayed to achieve a loading of 1.5mgcm^{-1}. The GDL was then dried in an oven for 1 hour at 60°C. The cell was fabricated using a polypropylene separator (Cellgaurd 5550).

The cell was assembled following the previous design specifications with approximately 2mL of 6M KOH (Sigma Aldrich). Full cell cycling was completed using recurrent galvanic pulses of 50mA. Each cycle consisted of 300 second discharge step followed by a 300 second charging step. Galvanodynamic testing was completed by scaling the current from 0 to 300mA at a rate of 5mA per second. Finally impedance measurements were completed from 100KHz to 0.1KHz at 500mV and 800mV.

4.3 Results and Discussion

Full cell testing of the new electrode design showed the need for an activation of the catalyst and electrode. This can easily be seen in Fig. 29, where the discharge potential starts off extremely low, at approximately 0.250V. The discharge potential improves inversely for some time, and stabilizes after approximately 100 full cycles. This supports is ideology of the need for activation of the catalyst and electrode. An activation phase of 50 cycles should be sufficient to overcome this poor initial performance of the new electrode design.

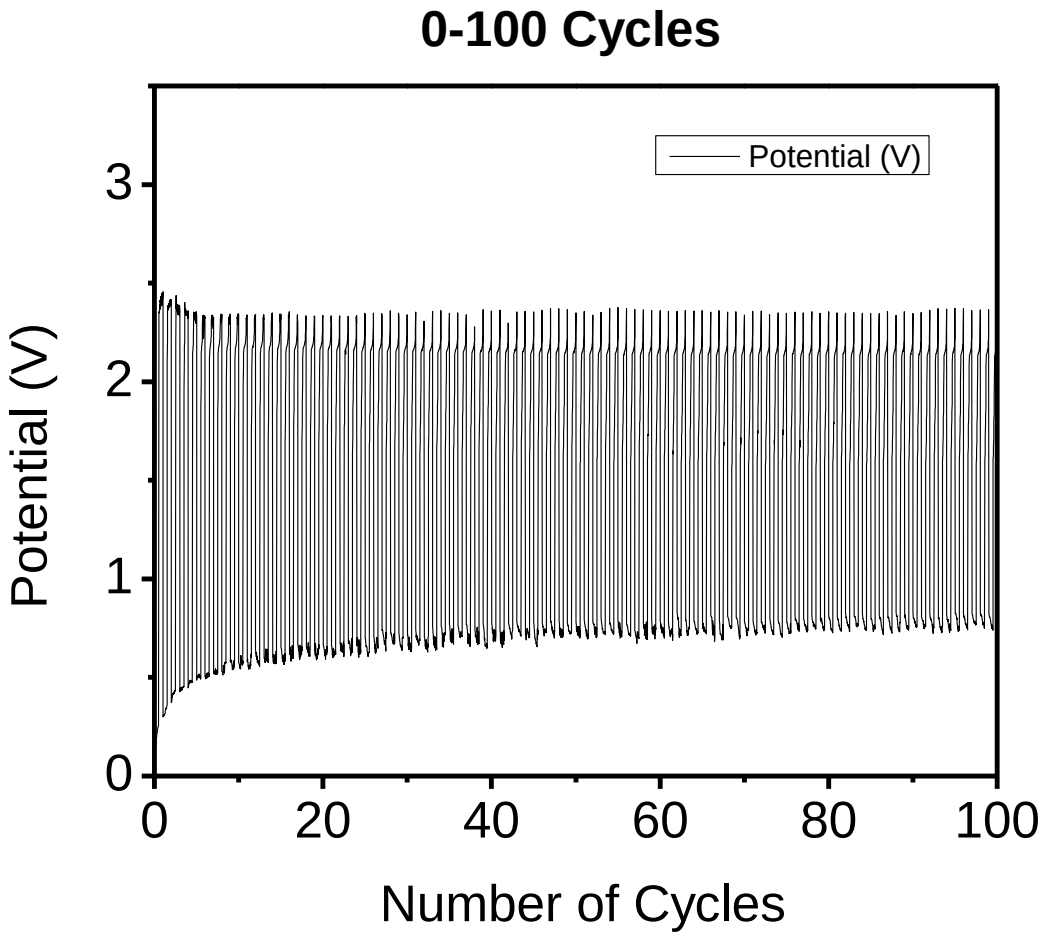

Figure 29: Full cell cycling of zinc air battery containing cobalt oxide nanowires brush coated on new electrode design. First 100 cycles

The electrode and catalyst performance continued to improve, more noticeably so in charging potential which was approximately 2.4V at the end of 100 cycles, but had significantly improved to between 2.15 and 2.22V between the 200th and 300th cycles. The discharge potential remained relatively consistent between 0.7V and 0.8V. This drop in discharge potential is proposed to have been cause due to the gradual accumulation of zinc hydroxide in the electrolyte of the cell. It is

proposed that initially the concentration of zinc hydroxide in solution is very low, which limits charging in terms of mass transport. This reduces charging efficiency and results in a higher potential for charging. As the cell is repeatedly cycled, the zinc hydroxide concentration gradually increases, due to inefficiencies in the cell, causing accumulation of zinc hydroxide.

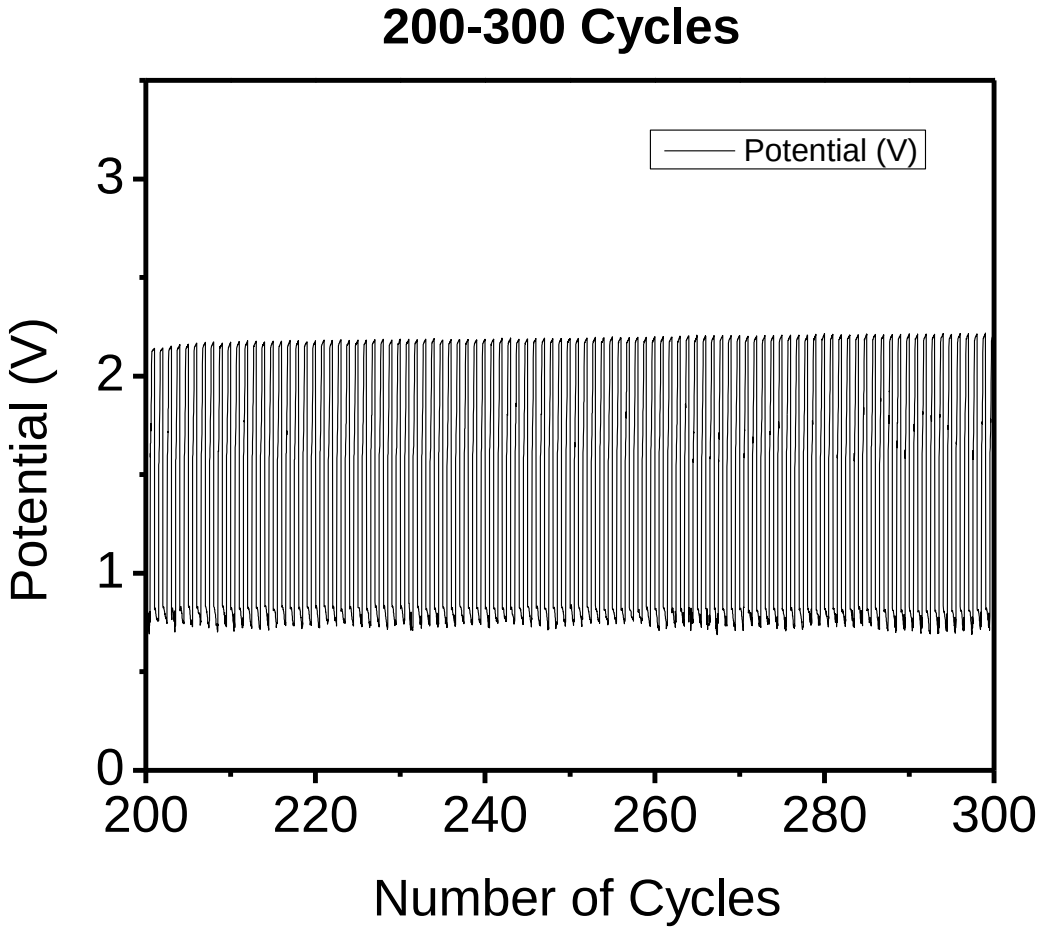

Figure 30: Full cell cycling of zinc air battery containing cobalt oxide nanowires brush coated on new electrode design. 200-300 cycles

After 600 cycles, the charging performance of the new electrode remains consistent and stable at approximately 2.15 V. This potential is unchanged for 400 cycles, with the charging potential

matching that of cycles 200-300, as seen in Fig. 30. The discharge potential has degraded slightly but remains at approximately 0.7V for the duration of the 100 cycles shown in Fig. 31.

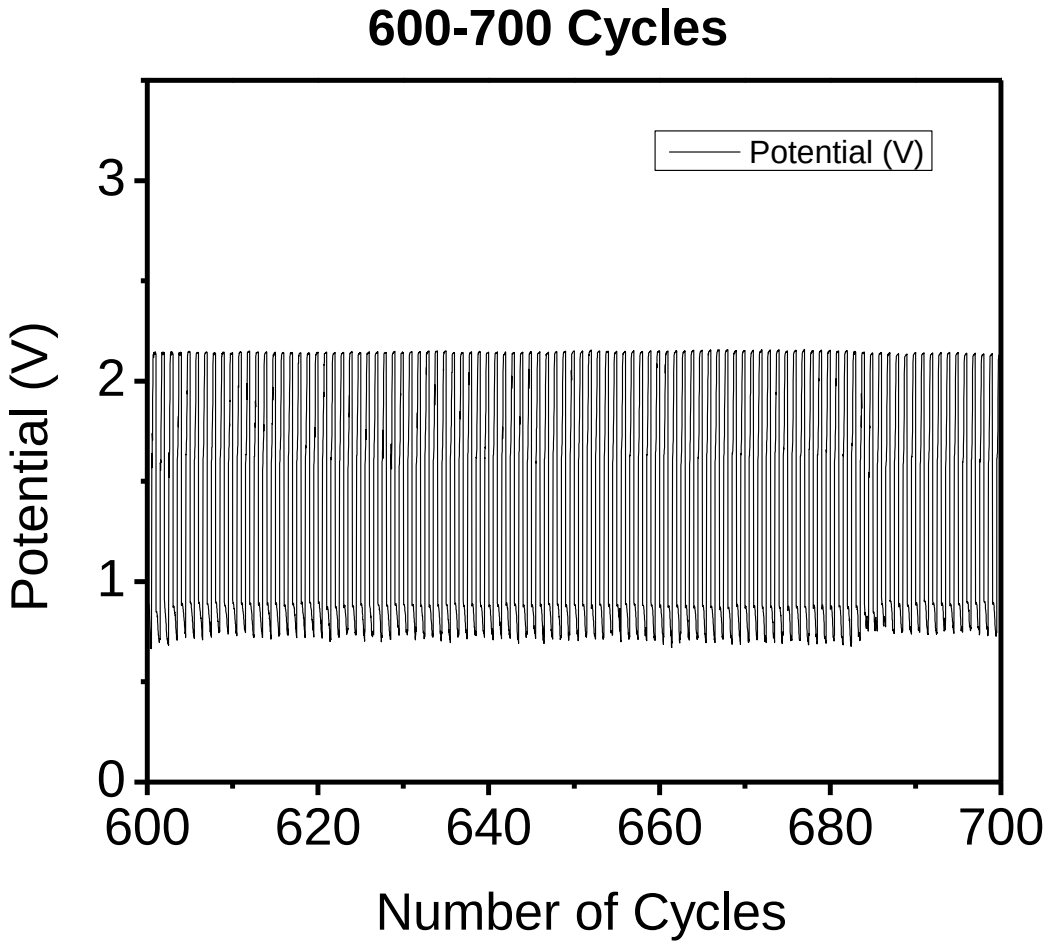

Figure 31: Full cell cycling of zinc air battery containing cobalt oxide nanowires brush coated on new electrode design. 600-700 cycles

The durability observed over the first 700 cycles of cell performance can be observed in Fig. 32. The new electrode design significantly outperforms the previous electrode design in which catalyst is loaded directly onto the amorphous carbon layer of the GDL. Most carbon based electrodes show significant performance decreases after 100 cycles. This can be specifically

exemplified by the platinum carbon performance which drops significantly after even 75 cycles, to less than 50% of the original discharge voltage observed in full cell testing [3]. The new electrode design shows consistent and durable performance, with no degradation in discharge performance over the initial 700 cycles of testing.

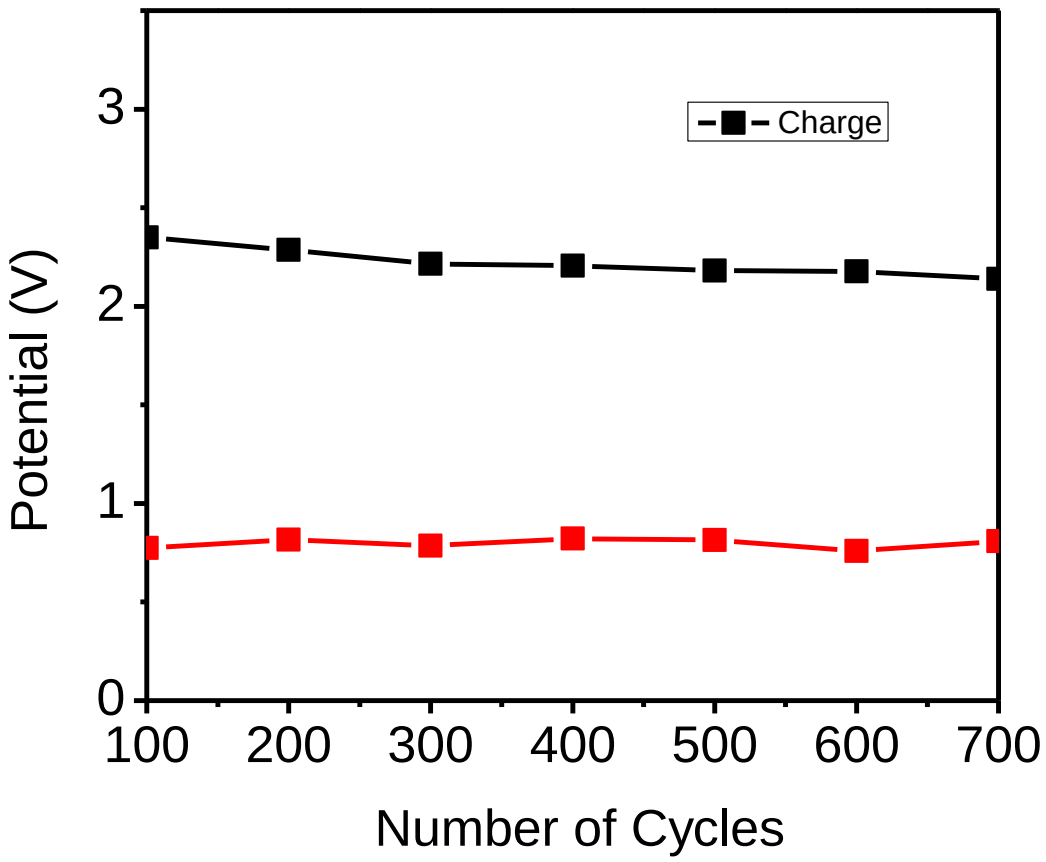

Figure 32: Full cell cycling of zinc air battery containing cobalt oxide nanowires brush coated on new electrode design. Overview of 700 cycles.

This discharge performance from this electrode was also slightly lower than that previously seen on standard carbon gas diffusion layers. It was thought that the brush coating used on the

stainless steel mesh caused agglomeration of the bifunctional catalyst, reducing the conductivity and active area of the cell. The same electrode was remade using a method of spray coating the catalyst onto the stainless steel mesh. The exact same loading was used for both methods of catalyst distribution onto the electrode. Similarly, identical full cell cycling testing methods were used. Fig. 33 illustrates the durability and high performance of this new electrode design. Each figure corresponds to 100 cycles of charge and discharge in succession.

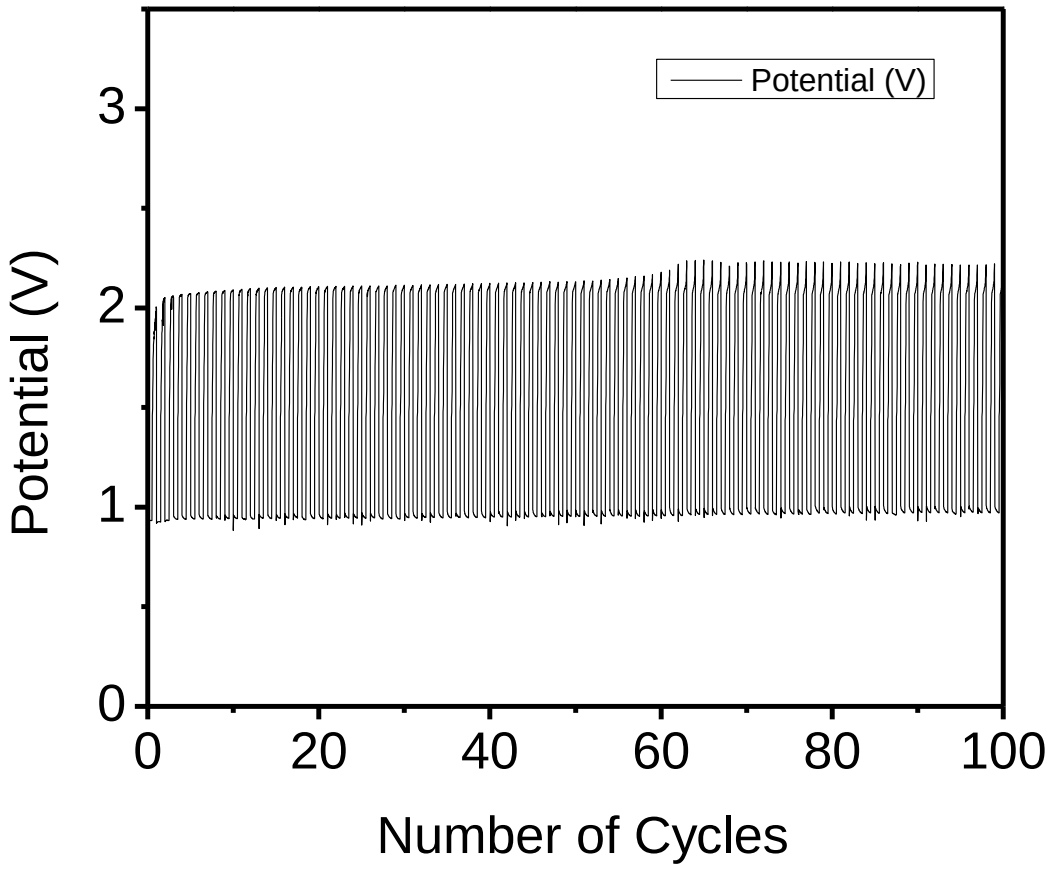

Figure 33: Initial 100 cycles of sprayed coated cobalt oxide nanowires on new electrode design

It was similarly observed that an activation phase of approximately 100 cycles was required for performance to stabilize. This activation phase may be viewable in Appendix A, in the group of figures labeled as full cycling charts for spray coated cobalt oxide on stainless steel. Fig. 34 shows the first 100 cycles after activation. The performance is significantly improved by comparison to the brush on method of catalyst coating. The charging potential is much lower between 2.07 and 2.19V compared to between 2.2 and 2.22V for the brush coated stainless steel GDL. More importantly a significantly higher discharge potential is observed, hovering around 0.95V compared to 0.75 for the brush coating. This higher performance can be consistently observed over 1000 cycles of repeating testing. This is due to the more even distribution of catalyst across the stainless steel mesh. When brush coating, the ink is applied thickly in some areas, causing some agglomeration or localized overloading in some areas of the electrode. Spray coating evenly coats the stainless steel in a thin layer of catalyst ink, resulting in better catalyst dispersion.

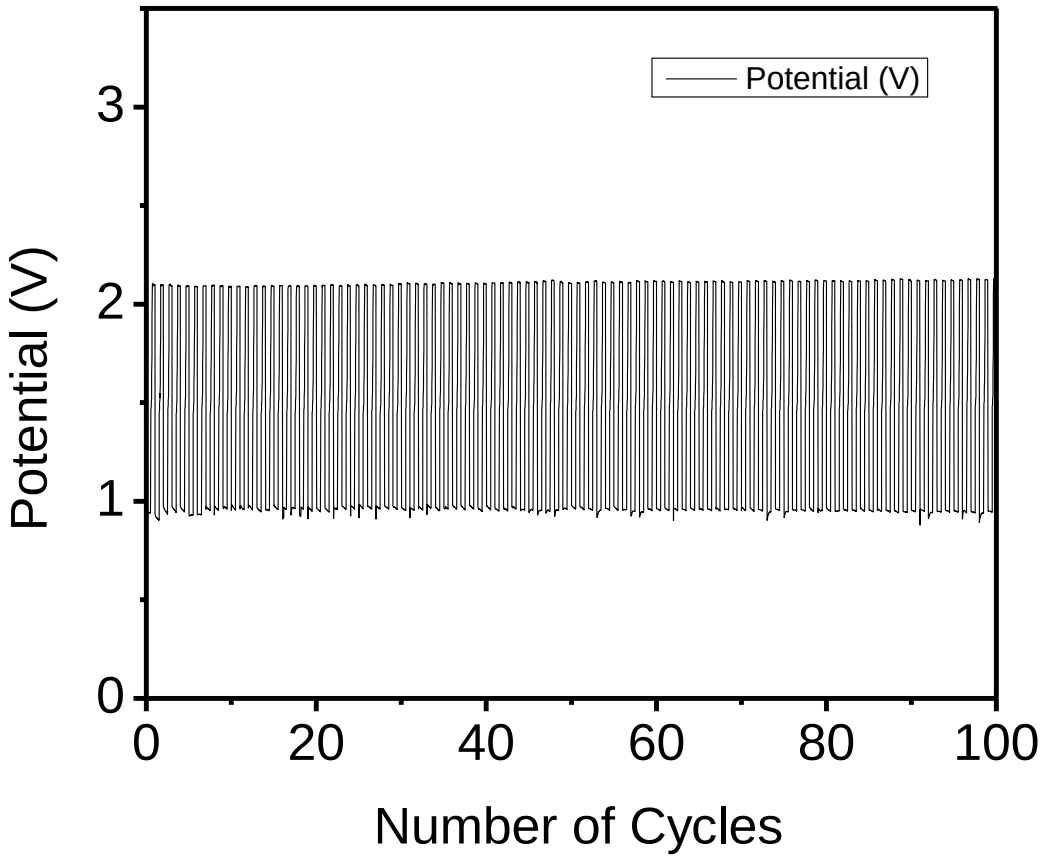

Figure 34: Cycles 900-1000 of sprayed coated cobalt oxide nanowires on new electrode design

The high durability of the new GDL can be observed by the consistent cycling for over 1000 cycles. The new GDL with spray on catalyst coating was able to cycle for over 1000 times with no degradation or decreases in performance after the initial 100 cycles of activation. The improved discharge and charging potentials seen on the spray coated sample suggest that brush coating indeed caused agglomeration or uneven distribution of the catalyst across the stainless steel mesh.

4.4 Conclusions

The project was successful in removing carbon dependency in gas diffusion layers. The issue of carbon corrosion was appropriately addressed, wherein the catalyst was bound directly to a stainless steel mesh via polymer binder Nafion^{TM}. Nafion^{TM} subsequently acted as a binder and an agent to increase the hydrophilicity of the catalyst layer in the GDL. Carbon corrosion was clearly not present as cycling was able to be carried out with no degradation for over 1000 cycles, compared to visible degradation after as little as 65 cycles with previous GDL types where the catalyst was bound to amorphous carbon. It was also shown that spray on coating of catalyst on the stainless steel mesh can drastically improve discharge and charging performance of the cell. Overall, the significant improvements in durability observed show promise for the commercial viability of zinc air batteries.

5.0 Improved Spinel Cobalt Oxide Morphology for Improved OER performance

5.1 Introduction and Purpose

Oxygen is utilized in the cell through two basic reactions, oxygen reduction (ORR) and oxygen evolution (OER). The kinetics of these reactions is slow however, and they require the use of a catalyst to progress at usable rates. Bifunctional catalysts which can catalyze both the OER and ORR reactions are therefore extremely beneficial, and are sought after for their use in zinc air batteries. The most effective bifunctional catalysts currently available are those based upon noble metals such as platinum. The high cost and limited availability of platinum and other precious metal catalysts are limiting the potential for zinc air batteries, and the need for low cost yet effective bifunctional catalysts is high. Groups of metal oxides such as spinels and perovskites have been proven to have good oxygen reduction abilities, and reasonable oxygen evolution potential, however there are still many issues with using them, mainly associated with the poor conductivity of metal oxides. This poor conductivity causes increase in impedance within the cell, and a higher oxygen evolution potential. This high oxygen evolution potential can cause hydrogen evolution and reduced efficiency of the cell. It is thought that by modifying the geometry of these spinel and perovskite structures, we can improve the OER performance and reduce cell impedance, hence improving the efficiency and overall performance of the cell.

5.2 Experimental

5.2.1 Synthesis Procedure

Two solutions are initially prepared, one containing 40mM cobalt nitrate, and one 100mM sodium hydroxide solution. The cobalt nitrate solution is placed in a three neck flak and purged with nitrogen for 30 minutes. The sodium hydroxide solution is then added drop wise while stirring the solution under ambient temperature. The resulting solution should change from pink to dark blue during this time in which the sodium hydroxide is added indicating utilization of the cobalt ions in solution, and the formation of cobalt oxide. The mixture is then removed from the flask and autoclaved at 180°C for 6 hours. The resulting residue is filtered and washed until pH is neutral, via acetone and water centrifugation. The sample is then calcined at 800°C for 4 hours in a nitrogen atmosphere. The schematic for this process can be seen by Fig. 35.

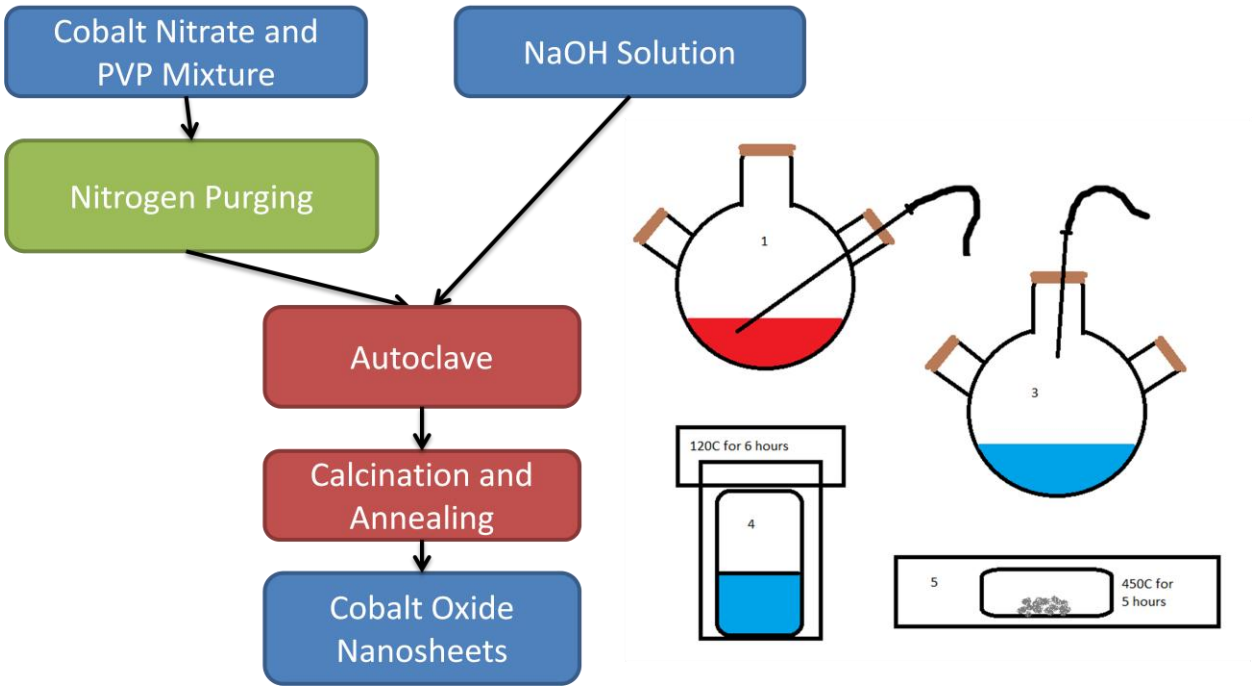

Figure 35: Schematic of synthesis procedure for cobalt oxide nanosheets.

5.2.2 Experimental Methods

Characterization was done on both particle and sheet morphology of spinel cobalt oxide via scanning electron microscopy (JEOL, Leo 1530). X-ray diffraction (XRD) analysis was completed (Bruker AXS D8 Advance) for both morphologies as well. Full cell battery testing was completed using in house fabricated acrylic cells, with the performance being analysed upon a multichannel potentiostat (Princeton Applied Research, VersaSTAT MC).

Prior to full cell testing, the air electrode was prepared by spray coating of a catalyst ink onto a carbon based gas diffusion layer. The ink was prepared by first mixing 10mg of catalyst into 1 mL of isopropyl alcohol. This mixture was then ultrasonicated for approximately 30 minutes before 67µL of 5wt% Nafion^{TM} solution was added. This Nafion^{TM} solution was created by diluting a stock 15wt% solution (Liquion Solution LQ-1115 1100EW 15 wt.%). The solution was further ultrasonicated for another 30 minutes before being spray coated onto the carbon gas diffusion layer (Ion Power Inc., SGL Carbon 10 BB, 2.5 cm×2.5 cm). The ink was sprayed to achieve a loading of 1.5mgcm-1. The GDL was then dried in an oven for 1 hour at 60°C. The cell was fabricated using a polypropylene separator (Cellgaurd 5550).

The cell was assembled following the previous design specifications with approximately 2mL of 6M KOH (Sigma Aldrich). Full cell cycling was completed using recurrent galvanic pulses of 50mA. Each cycle consisted of 300 second discharge step followed by a 300 second charging step. Galvanodynamic testing was completed by scaling the current from 0 to 300mA at a rate of 5mA per second. Finally impedance measurements were completed from 100KHz to 0.1KHz at 500mV and 800mV.

5.3 Results and Discussion

SEM techniques were used to analyse and investigate the morphology of both the spinel cobalt oxide nanoparticles and nanosheets. The cobalt nanosheets were investigated and found to have an approximate diameter of 400-500nm on average, with some sheets exceeding 700nm. These sheets were approximately 20-40nm thick on average. A multitude of pores can be seen on all facets of the cobalt oxide nanosheets, as shown in Fig. 36A. The nanosheets also display a relatively characteristic hexagonal shape, as seen in Fig. 36C and Fig. 36A. This shape can be seen on the vast majority of sheets present in the sample. The cobalt oxide nanoparticles were also analysed under SEM and found to be of a relatively uniform size at 20-40nm. Some particles were observed to be larger than 50nm in diameter. The nanoparticles were considerably smaller than the cobalt oxide nanosheet counterparts in this investigation. XRD analysis showed that both the cobalt oxide nanosheets and particles had the same crystal structure, as indicated by the matching of peaks to facets seen in Fig. 36D. All characteristic peaks of spinel cobalt oxide were identified and matched with the nanosheets and nanoparticles, indicating that our materials were true.

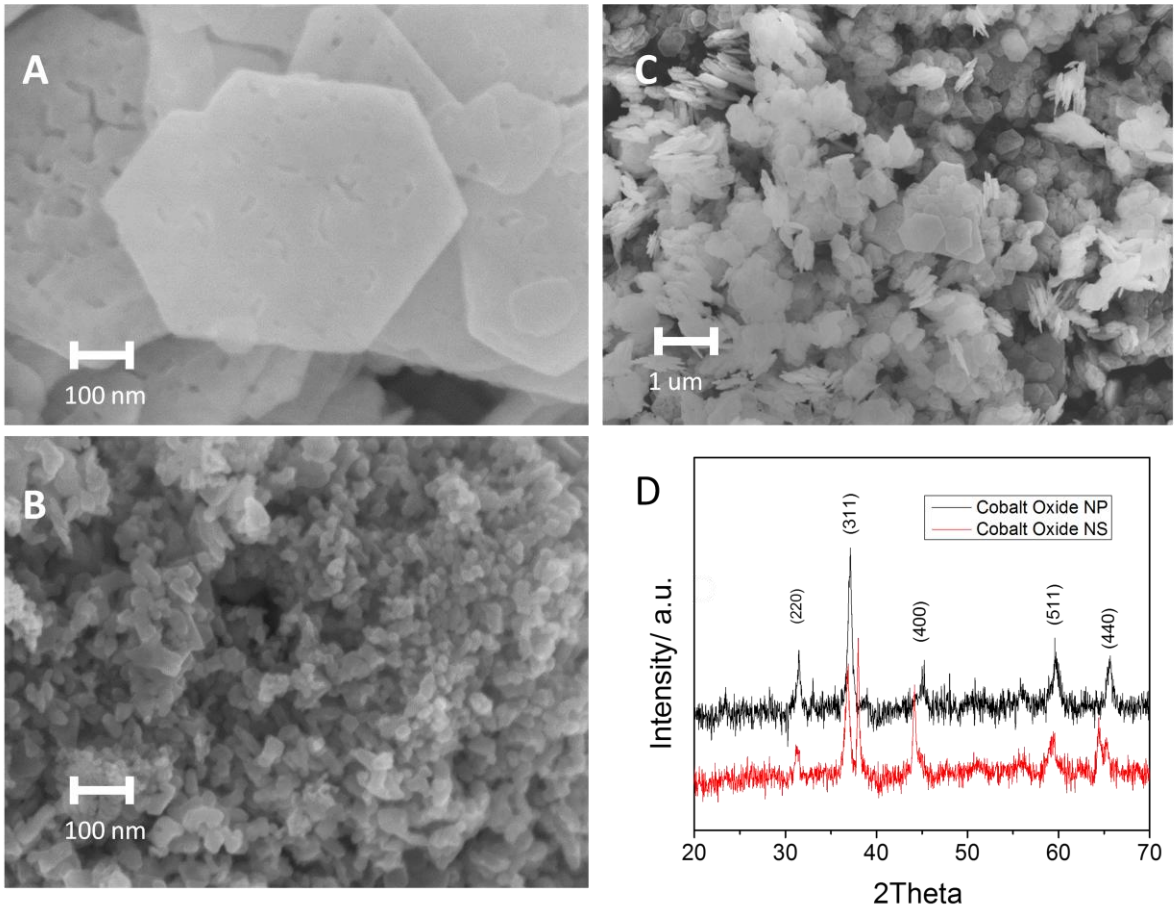

Figure 36: A) SEM Cobalt Oxide Nanosheets high magnification, B) Cobalt Oxide Nanoparticles high magnification, C) Cobalt Oxide Nanosheets lower magnification, D) XRD comparison of cobalt oxide nanoparticles and nanosheets.

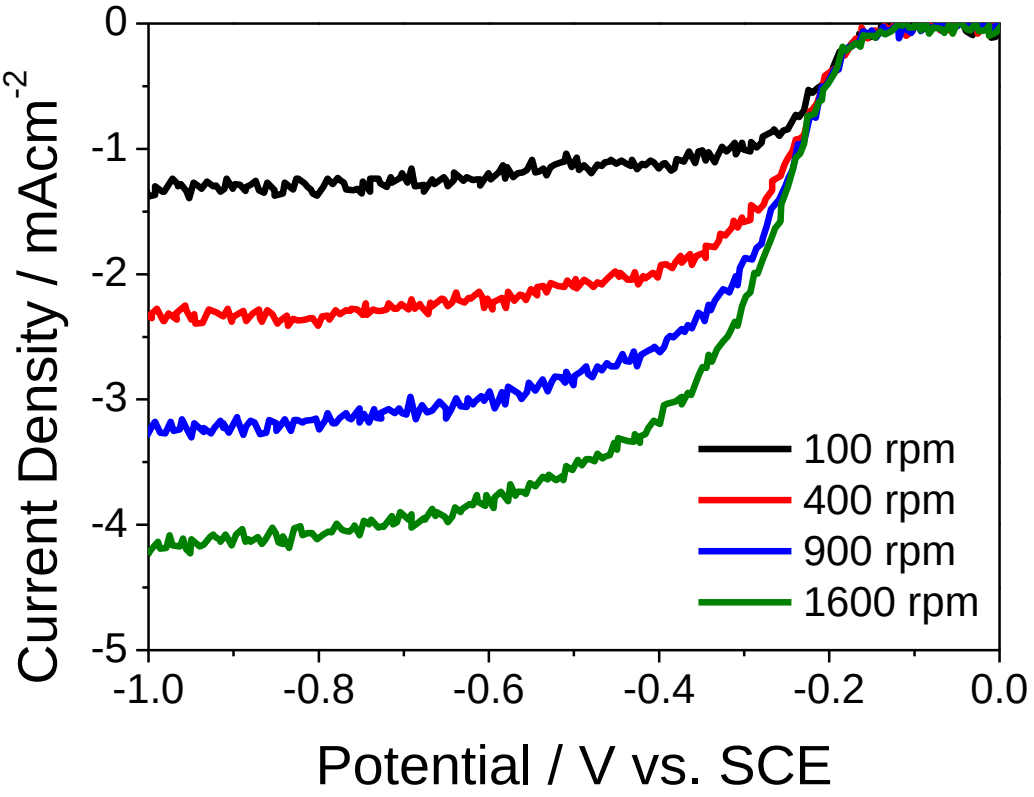

Figure 37: Linear Scan voltammetry for cobalt oxide nanosheets with graphene support.

The LSV data for cobalt oxide nanosheets on graphene carbon support is illustrated in Fig. 37. Four different rotation speeds were used, corresponding to four different rates of mass transfer to the working electrode. The nanosheets showed an extended diffusion or mass transport limited region, indicating strong ability of the catalyst to adsorb and release reactants and products. The half wave potential was observed to be approximately -0.27V, which is slightly low. This indicates somewhat poor or slower reaction kinetics.

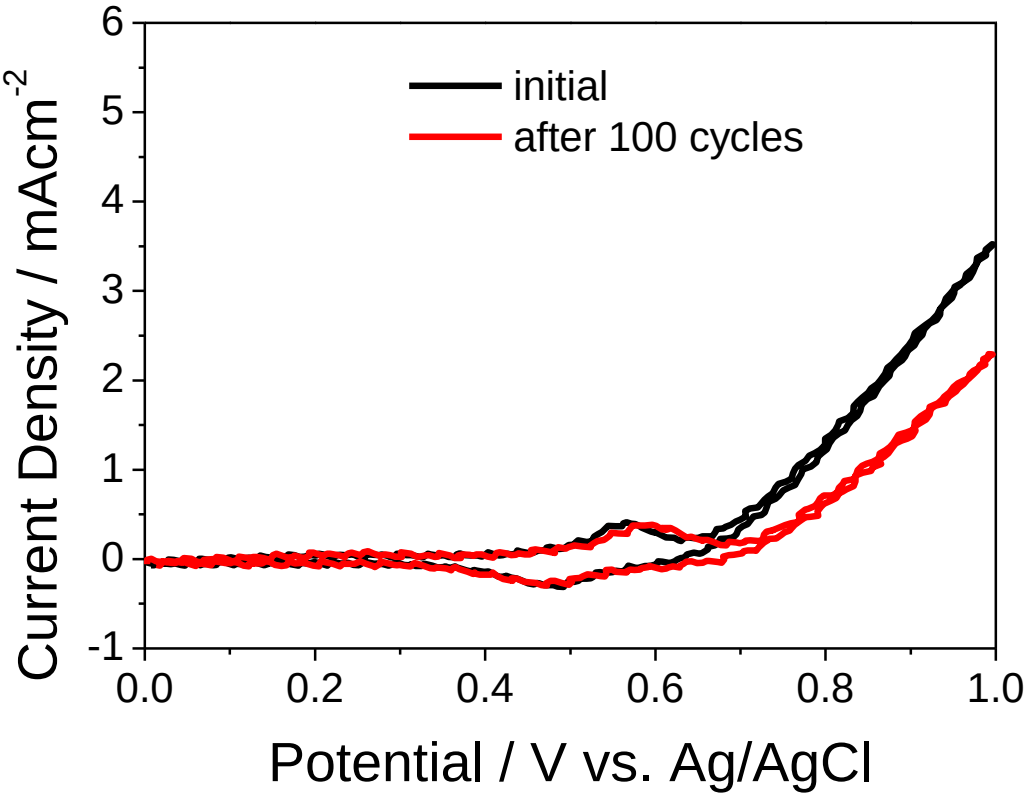

Figure 38: Cyclic voltammagram before and after 100 cycles for cobalt oxide nanosheets on graphene carbon support.

The high durability of cobalt oxide as a catalyst was quickly evident as seen in Fig. 38 where only a 31% decrease in current density was observed after 100 cycles. This low decrease in current density suggests strongly OER durability for cobalt oxide. This further illustrates and gives cause for full cell testing of cobalt oxide as an active OER and ORR catalyst. Full cell testing was completed on both cobalt oxide nanosheets and nanoparticles to compare directly on full cell performances the effects of morphology on OER and ORR performance and durability.

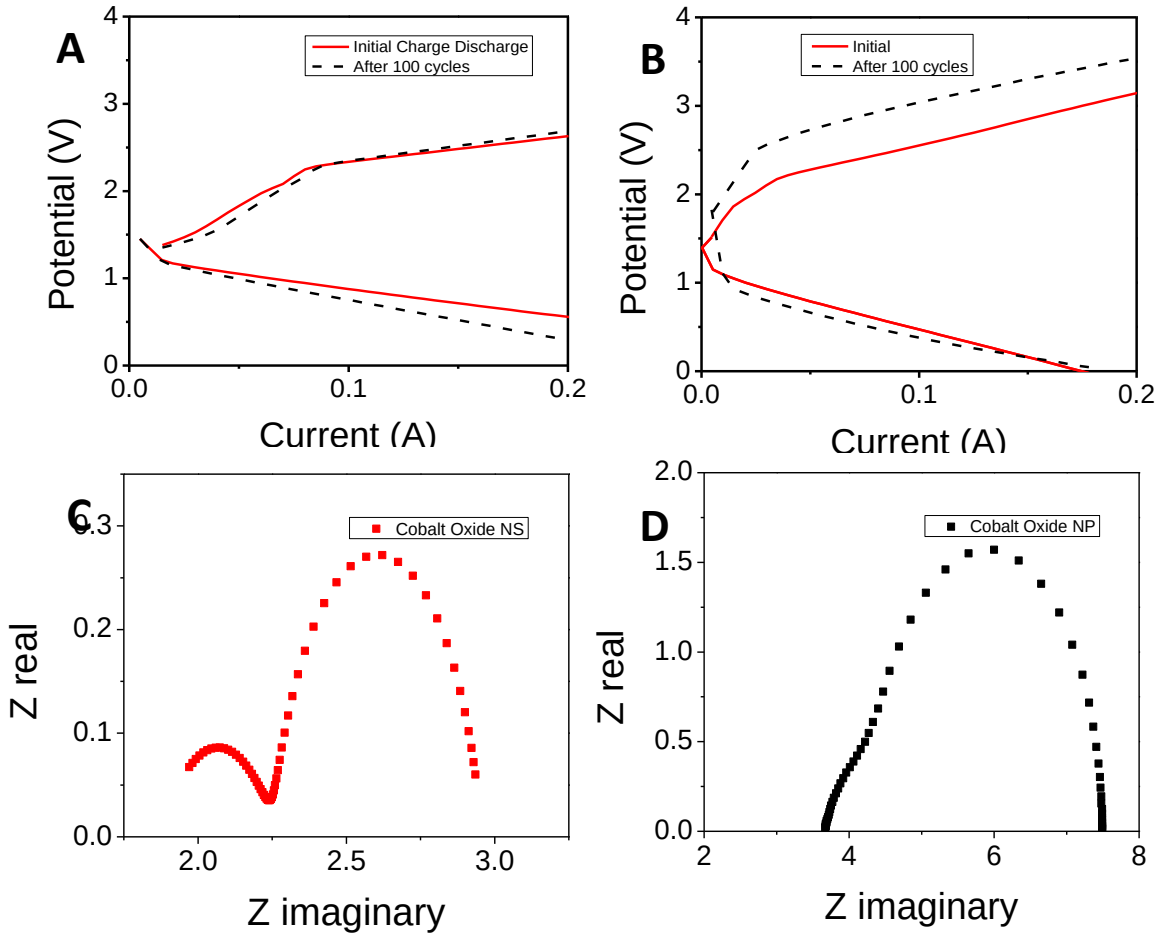

Figure 39: A) before and after 100 cycles galvanodynamic charge discharge for cobalt oxide nanosheets, B) before and after 100 cycles galvanodynamic charge discharge for cobalt oxide nanoparticles.C)Impedence analysis for cobalt oxide nanosheets, D)Impedence analysis for cobalt oxide nanoparticles

It can be seen from Fig. 39A and 39B that cobalt oxide nanosheets have improved charge and discharge potentials over nanoparticles, when exposed to the same glavanodynamic tests. Cobalt oxide nanosheets also exhibit improved durability, wherein after 100 cycles the nanosheets have retained most of the initial performance for charge and discharge potentials, while the charging potential for nanoparticles as decreased dramatically over cycling. This can be further illustrated by the comparison in Table 5 and Table 6.

Table 5: Comparison of cobalt oxide nanoparticle and nanosheet discharge potentials at various currents

Current	Potential NS initial	Potential NS 100 cycles	Potential NP initial	Potential NP 100 cycles
100mA	0.92V	0.86V	0.50V	0.46V
150mA	0.77V	0.56V	0.21V	0.21V
200mA	0.60V	0.27V	0V	0V

At higher currents of around 200 mA, the cobalt oxide nanosheets are still functioning while the nanoparticles stopped.

Table 6: Comparison of cobalt oxide nanoparticle and nanosheet charge potentials at various currents

Current	Potential NS initial	Potential NS 100 cycles	Potential NP initial	Potential NP 100 cycles
100mA	2.29V	2.29V	2.49V	3.06V
150mA	2.45V	2.58V	2.77V	3.25V
200mA	2.59V	2.62V	3.05V	3.45V

Similarly higher performance from cobalt oxide nanosheets is observed with chargin potentials. Nanosheets display more durable and lower charge potentials than their nanoparticle counterparts at all currents.

Electrochemical impedance spectroscopy was performed to identify causes for the higher performance observed by nanosheets. This improved performance can be explained by the generally lower impedance values observed from cobalt oxide nanosheets seen by Fig. 39C and 39D. The nyquist plots clearly show that both nanosheets and particles have two semicircles at high and low frequencies. These plots were fitted to an equivalent circuit to further investigate the electrode process [44, 45]. R_s represents the resistance associated with cell components. This includes but is not limited to the resistance in contact and conductivity of various components such as the current collector. R_{int} represents the interface resistance between the catalyst and

electrolyte. R_{ct} relates to the charge transfer resistance which occur during reaction kintetics [44, 45]. Finally, Q_{dl} is the double layer capacitance and Q_{int} relates to the solid electrolyte interphase capacitance. The equivalent circuit components for nanoparticles and nanosheets are presented in Table 7.

Table 7: Equivalent circuit elements and respective values for cobalt oxide nanoparticles and nanosheets in full cell testing

Resistance	R_s	R_{int}	R_{ct}	Q_{int}	Q_{dl}
Nanosheets	1.875	0.3835	0.6977	0.005145	0.1974
Nanoparticles	3.663	0.8607	2.972	0.003125	0.001647

The overall battery resistance shown by R_s are much smaller for cobalt oxide nanoparticles. This implies better conductivity of the active layer, which is one of theories as to the higher OER performance from nanosheets. The R_{ct} values for cobalt oxide nanosheets are also much smaller than that on nanoparticles. This indicates that nanosheets are more efficient at ORR reactions, compared to nanoparticles.

Fig. 40. illustrates the full cell performance of both cobalt oxide nanoparticles and nanosheets over 75 galvanostatic cycles.

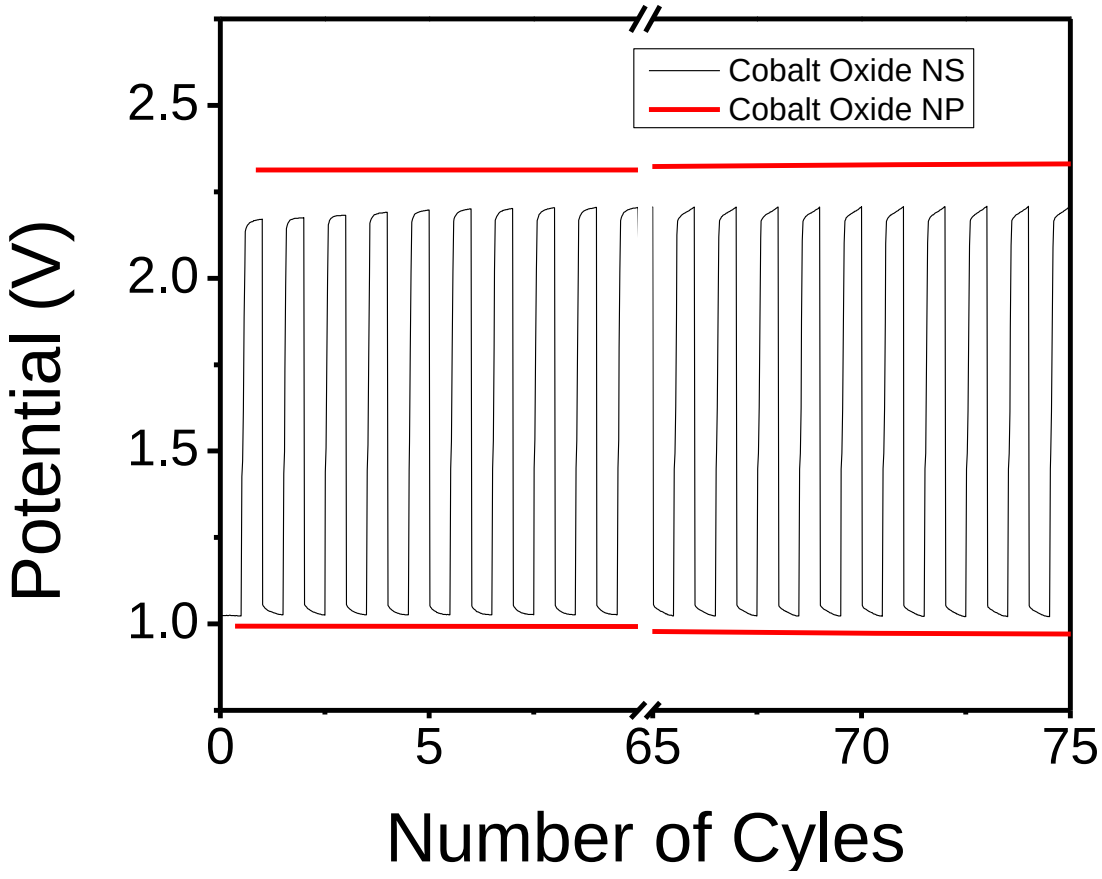

Figure 40: A) Full cycling comparison of Cobalt Oxide Nanosheets and nanoparticles, 1.5 mg/cm^{-1} catalyst loading, 50mA current.

As expected from the half-cell cyclic voltammertry data, the durability of cobalt oxide was observed to be quite high, with only a 2% loss in both charge potentials for both cobalt oxide nanoparticles and nanosheets. Similarly only a 2% loss in discharge potential was lost after 75 cycles for cobalt oxide nanosheets, and 5% loss in discharge potential for cobalt oxide nanoparticles. It was observed that cobalt oxide nanosheets had a significantly lower discharge potential on average of 2.18V compared to 2.3V for cobalt oxide nanoparticles. This is over 100mV which corresponds to significant improvement in efficiencies. If the charging cycle was

not galvanostatic, such as in real world applications, the current required at a specific voltage increase exponential with increase over potentials required for charging. This means even small improvements in the charging or OER potentials can have significant improvements on the charging efficiency of the battery. Similar to the improved comparative performance of cobalt oxide nanosheets to nanoparticles for charging potentials, cobalt oxide nanosheets demonstrated higher discharge potential than cobalt oxide nanoparicles for the entirety of the 75 cycles. The durability of cobalt oxide nanosheets also appears to be greater than nanoparticles in that the discharge potential of the nanoparticles decreases more over the extended cycling. The difference in discharge voltage between nanosheets and nanoparticles increases over time. By extrapolation it can be assumed that with more cycling the difference in performance between cobalt oxide nanoparticles and nanosheets would be even more evident. One explanation for the higher performance associated with nanosheet morphology is the overlapping nature and better connection between plates, rather than the poor connection associated with contact between particles. The thickness of nanosheets created are approximate the same as the diameter of the nanoparticles, 20-40nm. This means that the cross through distance between a nanoparticle and nanosheet is the same. This indicates that improvements in conductivity cannot be interpreted by thickness of oxide coating or distance in which current has to travel through the semiconducting oxides.

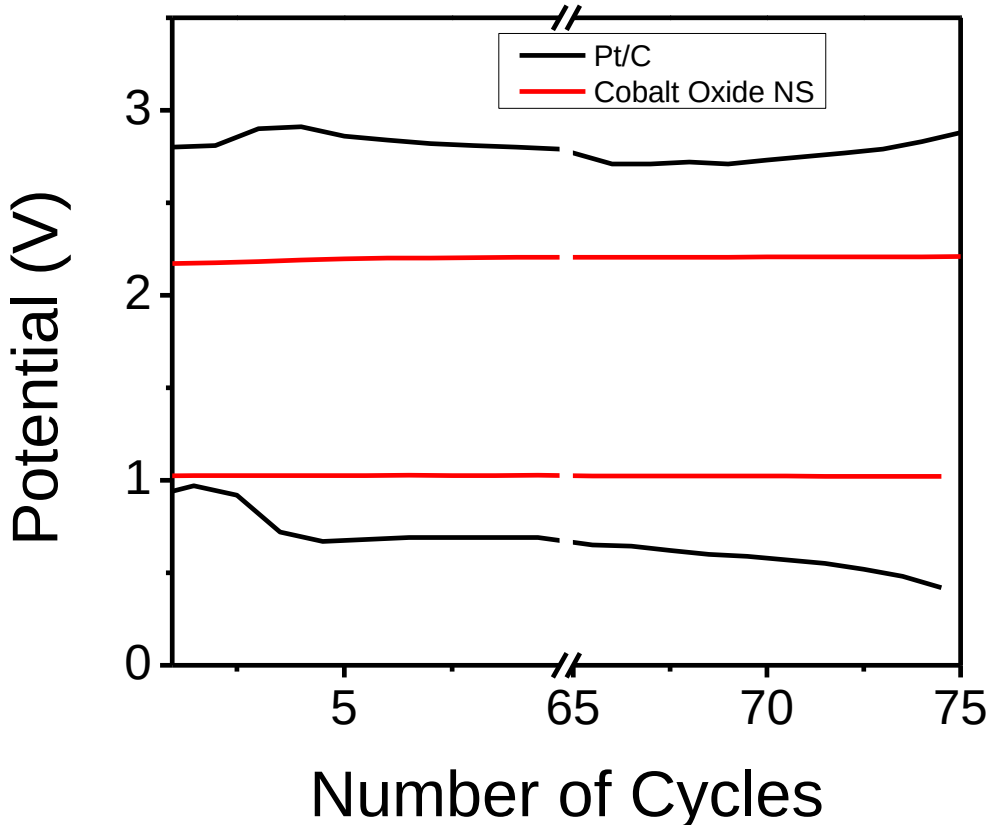

Figure 41: Full cycling comparison of cobalt oxide nanosheets to platinum carbon 1.5mgcm^{-1} loading for both catalysts

Platinum carbon is one of the better performing precious metal catalysts, and is often a benchmark in fuel cell and battery testing. In terms of full cell cycling, cobalt oxide nanosheets outperformed platinum carbon in every way. A comparison of platinum carbon to cobalt oxide nanosheets is visible in Fig. 41. The discharge potentials start similar, with cobalt oxide nanosheets still demonstrating higher discharge potentials, however after very few cycles the platinum discharge potential drops to just over 700mV, while the cobalt oxide nanosheets remain slightly above 1.0V. Similarly the cobalt oxide nanosheets outperforms the platinum carbon

significantly in terms of charging potential. The overall potential comparison can be viewed in Table 8.

Table 8: Comparison of initial and post 75 cycles charge and discharge potentials for Pt/C, Commercial Primary Zinc air Catalyst, and Cobalt Oxide Nanosheets

Pt/C20 wt %		Co3O4 Nanosheets	
Initial (V)	After 75 (V)	Initial (V)	After 75 (V)
0.95	0.42	1.02	1.02
2.75	2.86	2.17	2.19

5.4 Conclusions

Cobalt oxide nanosheets very successfully synthesised with a thickness of 20-40nm, comparable to the diameter of cobalt oxide nanoparticles used for testing. Half-cell testing showed promising durability under Zn air operational conditions and as such results indicating that cobalt oxide nanosheets have potential for bifunctional catalysis. Galvanodynamic testing showed that cobalt oxide naosheets have higher performance that nanoparticles in the areas of charge potential, discharge potential, and durability. Electrochemical impedance analysis showed that cobalt oxide nanosheets are more conductive than nanoparticles when operating in full cell. Additionally, the cobalt oxide nanosheets appear to be more efficient catalysts due to the lower charge transfer resistance. Cobalt oxide nanosheets again show better durability when tested by full cell cycling when compared to nanoparticles. These reasons elevate the nanosheet morphology above that of nanoparticles as bifunctional catalysts of cobalt oxide. The cobalt oxide nanosheets were further

compared to an industry benchmark bifunctional catalyst, platinum carbon. The cobalt oxide nanosheets also outperformed that platinum carbon in discharge potential, charging potential as well as durability. Where that platinum carbon had lost 51% of its discharge potential after 75 cycles, the discharge potential for cobalt oxide nanosheets was degraded by 0%.

6.0 Summary and Future Work

6.1 Conclusions

In summary, zinc air batteries are currently limited by several major issues, three of which have been addressed with solutions in this thesis. One major problem is the lack of well designed high surface area zinc anodes, which maintain high structural integrity, conductivity, and controlled porosity. Another major issue is the poor durability of gas diffusion electrodes, wherein corrosion of the supporting carbon can cause loss of catalyst and in turn, performance. The third major issue addressed was the lack there of stable, durable, high performance non precious catalysts. The three studies addressing these issues are highlighted and this work investigated potential solutions to this challenges. These studies help to provide future direction from zinc air batteries as a technology, solving many scientific problems associated with their commercial viability.

The first study addresses the issue of high surface area anode design. Current porous zinc anode designs use zinc powders or fibers which are gelled or bundled together to form the anode. Zinc powders have a higher surface area but extremely poor interconnectivity of particles, and in turn high internal resistances. Additionally they are limited in porosity due the particle nature in the sense that over spacing the particles cause a steep drop in conductivity. The proposed procedure for porosity controlled high surface area anodes follows an ideology in which a filler compound is mixed with zinc and pressed at moderate pressure. This pellet is heated to cause the filler to sublime, and anneal the zinc, leaving a porous structure. This porous anode demonstrated

significantly improved charge discharge performance over zinc plates as shown by galvanodynamic analysis. An increase in discharge potential of up to 200% was found, with a decrease in charging potential of up to 58%. This ease of fabrication and porosity controlled method is easily scalable and environmentally benign, warranting promise for higher capacity and better performing zinc air batteries.

The second study focuses on addressing issues of durability pertaining to the gas diffusion electrode. The issue of carbon corrosion was addressed by polymer binding catalyst directly to a stainless steel current collector. The hydrophilic nature of the amorphous carbon layer was maintained by pressing a layer of amorphous carbon with PTFE treated carbon fiber to the back of the current collector. Significant improvements in durability were noted, wherein previous zinc air cells were capable of running of a few hundred cycles before significant reduction in performance [3], the new proposed electrode was able to run with no loss in performance for over 1000 cycles. These outstanding results show a strong outlook for zinc air batteries in term of coming closer to commercial standards for cycling durability.

The third study focuses on improving cobalt oxide morphology for the use as a high performance and highly durable bifunctional catalysts, ideally to be competitive with benchmark platinum carbon. Cobalt oxide nanosheets were successfully synthesized and first compared to cobalt oxide nanoparticles by glavanodynamic charge discharge testing and electrochemical impedence analysis. The cobalt oxide nanosheets showed significantly higher performance in terms of charge and discharge potentials, as well as increased durability to cycling. From impedance

analysis it was determined that the cobalt oxide nanosheets were indeed more efficient at performing oxygen reduction reactions than the nanoparticle counterparts. Additionally, the nanosheets were shown to have better conductivity when applied to full cell testing. The cobalt oxide nanosheets where then compared to platinum carbon and were significantly more durable. Additionally, the cobalt oxide nanosheets showed lower charging potentials, and higher discharge potentials, both relating to better performance. These results show promise that nonprecious bifunctional catalyst can be made to replace precious metal catalysts in the future, which would bring zinc air batteries much closer to commercial feasibility.

Together these studies show that improvement of metal air, specifically Zn air technology, is possible, opening up numerous possibilities in applications for zinc air batteries to various energy storage systems.

6.2 Future Work

The three investigations provided insight into solutions to problems pertaining to three major components of zinc air batteries; the zinc anode electrode, the gas diffusion electrode, and the bifunctional cathode catalyst. However, many future directions are possible with this new knowledge.

1. Pertaining to the zinc electrode, the incorporation of zinc allows into the design would address other problems associated with anode function, such as dendrite formation and stability. In addition to the incorporation of zinc alloys, study could be done on the incorporation of a copper foam or mesh structure underlying the zinc structure, in order to further reduce dendrite formation, and improve durability. A study is recommended in order to quantify the impact of method

preparation parameters such as zinc and filler compound particle size on pore size, and to correlate pore size with performance. This study could take the form of a ‘Design of Experiment’ experimental design.

2. Pertaining to the gas diffusion electrode, the replacement of the Nafion™ binder with more conductive polymer binders or binders solution ‘doped’ with graphene would further improve overall cell resistance, and possibly increase durability further. Similarly so, durability could possibly be further increased by replacing the amorphous carbon layer with hydrophilic type polymers. Investigation should be done into the effects of these perceived improvements

3. Pertaining to the bifunctional catalyst, further investigation could be done into various morphologies of cobalt oxide, such as nanowires, nanocubes, and other various structures. Additonally, the nanosheet structure should be analysed for other types of semiconducting spinel oxides, in order to see if the morphology improvements observed in cobalt oxide are applicable to other materials.

References

[1] Jolley, A. **2006**, The Supply of Fossil Fuels. Climate Change Working Paper No.9.

[2] Tahil, W. **2007**, The Zinc Air Battery and the Zinc Economy.

[3] Zhu Chen, A.; Y.,Ahmed R, Wang H,; Li H, Zhongwei Chen, *Electrchimica Acta* **2012,** *69*, 295-300.

[4] Battery Energy Density Comparison. http://www.iccnexergy.com/battery-energy-density-comparison/ (accessed April 1).

[5] Chen, Z. **2012**. Nitrogen-Doped Carbon Materials as Oxygen Reduction Reaction Catalysts for Metal-Air Fuel Cells and Batteries. Chemical Engineering, University of Waterloo. **MASc**.

[6] B. Scrosati, J. Garche, *Journal of Power Sources* **2010,** 195, (9), 2419-2430.

[7] G. Girishkumar, B. McCloskey, A. Luntz, S. Swanson, W. Wilcke, *Journal of Physical Chemistry Letters* **2010,** 1, (14), 2193-2203.

[8] A. Kraytsberg, Y. Ein-Eli, *Journal of Power Sources* **2011,** 196, (3), 886-893.

[9] R. Padbury, X. W. Zhang, *Journal of Power Sources* **2011,** 196, (10), 4436-4444.

[10] T. Ogasawara, A. Debart, M. Holzapfel, P. Novak, P. G. Bruce, *Journal of the American Chemical Society* **2006,** 128, (4), 1390-1393.

[11] J.S. Lee, S. T. Kim, R. Cao, N. S. Choi, M. Liu, K. T. Lee, J. Cho, *Advanced Energy Materials* **2011,** 1, (1), 34-50.

[12] J. Goldstein, I. Brown, B. Koretz, *Journal of Power Sources* **1999,** 80, (1-2), 171-179.

[13] T. Reddy, D. Linden, *Linden's Handbook of Batteries*. McGraw-Hill: **2010**.

[14] F. R. Mclarnon, E. J. Cairns, *Journal of the Electrochemical Society* **1991,** 138, (2), 645-664.

[15] S. Zhu , Z. Chen , B. Li , D. Higgins , H. Wang , H. Li , Z. Chen , *Electrochem. Acta* **2011** , *56* , 5080 .

[16] S. Shanmugam , T. Osaka , *Chem. Commun.* **2011** , *47* , 4463 .

[17] S. Yang , X. Feng , X. Wang , K. Mullen , *Angew. Chem. Int. Ed.* **2011** , *50* , 5339 .

[18] W. Yang , T.P. Fellinger , M. Antonietti , *J. Am. Chem. Soc.* **2010** , *133* , 206.

[19] W. Li , A. Yu , D. C. Higgins , B. G. Llanos , Z. Chen , *J. Am. Chem.*

Soc. **2010** , *132* , 17056 .

[20] J.S. Lee , T. Lee , H.K. Song , J. Cho , B.S. Kim , *Energy Environ. Sci.* **2011** , *4* , 4148 .

[21] F. Cheng , J. Shen , B. Peng , Y. Pan , Z. Tao , J. Chen , *Nat. Chem.* **2011** , *3* , 79 .

[22] Y. Gorlin , T. F. Jaramillo , *J. Am. Chem. Soc.* **2010** , *132* , 13612 .

[23] Z. Yang , X. Zhou , H. Nie , Z. Yao , S. Huang , *ACS Appl. Mater. Interfaces.* **2011** , *3* , 2601 .

[24] Y. Qian , S. Lu , F. Gao , *Mater. Lett.* **2011** , *65* , 56 .

[25] K. Gong , P. Yu , L. Su , S. Xiong , L. Mao , *J. Phys. Chem. C* **2007** , *111* , 1882.

[26] J. Lee , G. Park , H. I. Lee , S. Kim , R. Cao , M. Liu , J. Cho , *Nano Lett.* **2011** , *11* , 5362 .

[27] Yang, C. C.; Lin, S. J. *Journal of Power Sources* **2002,** 112, (1), 174-183.

[28] N.C. Tang, US Patent 6,221,527 B1 **2007**.

[29] Chang Woo Lee, K. S., Seung Wook Eom, Hyun Soo Kim, Mun Soo Yun *Journal of Power Sources* **2006**, 159, 1474

[30] Chang Woo Lee, K. S., Seung Wook Eom, Mun Soo Yun, *Journal of Power Sources* **2006,** 160, 1436-1441.

[31] Y. Bing , H. Liu , L. Zhang , D. Ghosh , J. Zhang , *Chem. Soc. Rev.* **2010**, *39* , 2184 .

[32] V. R. Stamenkovic , B. Fowler , B. S. Mun , G. Wang , P. N. Ross , C. A. Lucas , N. M. Markovi , *Science* **2007** , *315* , 493 .

[33] J. Greeley , I. E. L. Stephens , A. S. Bondarenko , T. P. Johansson , H. A. Hansen , T. F. Jaramillo , J. Rossmeisl , I. Chorkendorff , J. K. Norskov , *Nat. Chem.* **2009** , *1* , 552.

[34] V. Neburchilov, H. Wang, Jonathan J. Martin, Wei Qu, *Journal of Power Sources* **2010,** *195*, 1271-1291.

[35] S.B. Kanungo, K.M. Parida, B.R. Sant, Electrochim. Acta **1981,** 26, 1157.

[36] S. Liompart, L.T. Yu, J.C. Mas, A. Mendiboure, R. Vignaud, J. Electrochem. Soc. **1990,** 137, 371.

[37] K. Matsuki, H. Kamada, Electrochim. Acta **1986,** 31, 13.

[38] W.A Armstrong, US Patent 3,948,684 **1976**.

[39] N. Koshiba, H. Hayakawa, K. Momose, A. Ohta, US Patent 4,595,643 **1984**.

[40] J. Vondrak, B. Klapste, J. Velicka, M. Sedlarikova, R. Cerny, J. Solid State Electrochem. **2003,** 8, 44.

[41] H. Meng, P.K. Shen, Electrochem. Commun. 8 (2006) 588.

[42] K. Kinoshita, Carbon, John Wiley & Sons Inc., New York, 1988.

[43] A.C. Tseung, S. Jasem, Electrochim. Acta **1977**, 22, 31.

[44] G.Q. Zhang, X.G. Zhang, H.L. Li, J. *Solid State Electrochem*. **2006**, 10, 995.

[45] D. Thiele, A. Zuttel, J. *Power Sources* **2008**, 183, 590.

Appendix

Published papers are used in the thesis. The permissions to reuse the published results have been granted by the Publisher. Below are the License numbers from the Publishers.

Elsevier Publishing, 3120250343241, 3134951378752

Below are a series of figures illustrating the durability of the new gas diffusion electrode design. Each figure represents 100 cycles of galvanodynamic testing, totaling 1000 cycles.

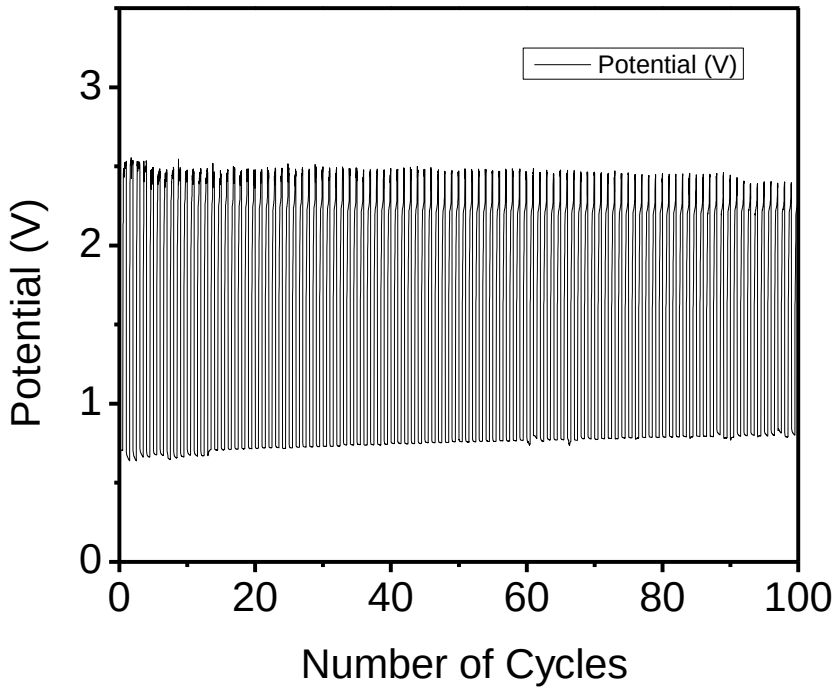

Figure 42: Initial 100 cycles, cobalt oxide nanowires spray coated on stainless steel mesh gas diffusion layer

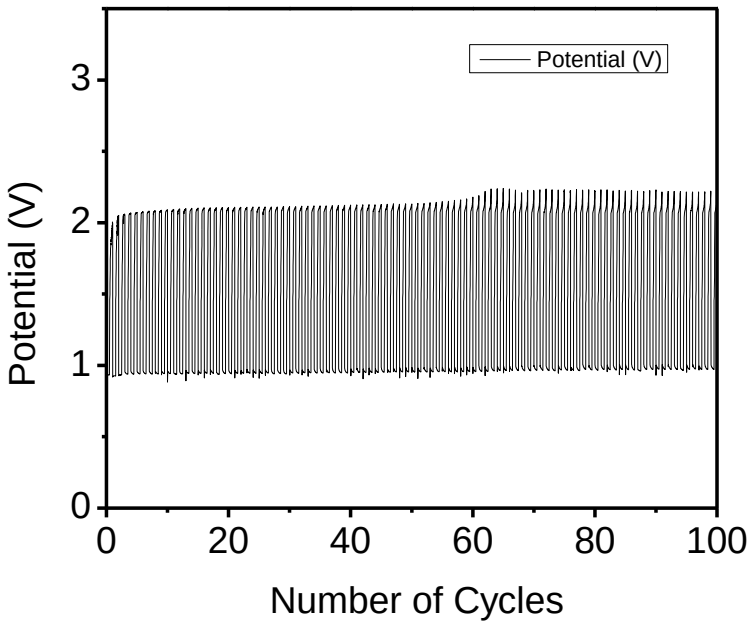

Figure 43: 100-200 cycles, cobalt oxide nanowires spray coated on stainless steel mesh gas diffusion layer

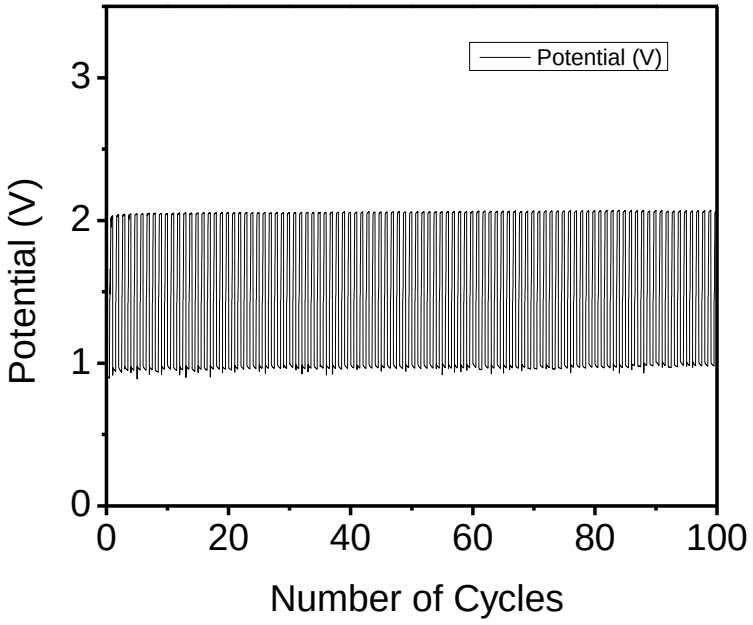

Figure 44: 200-300 cycles, cobalt oxide nanowires spray coated on stainless steel mesh gas diffusion layer

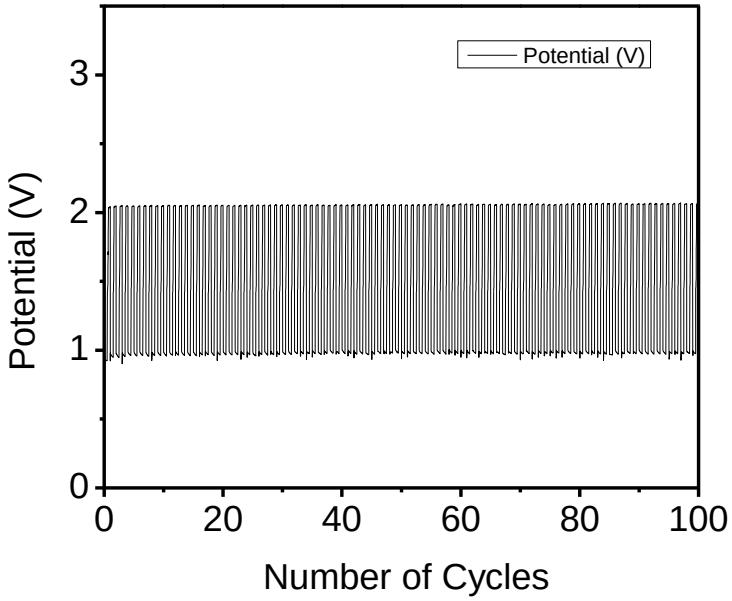

Figure 45: 300-400 cycles, cobalt oxide nanowires spray coated on stainless steel mesh gas diffusion layer

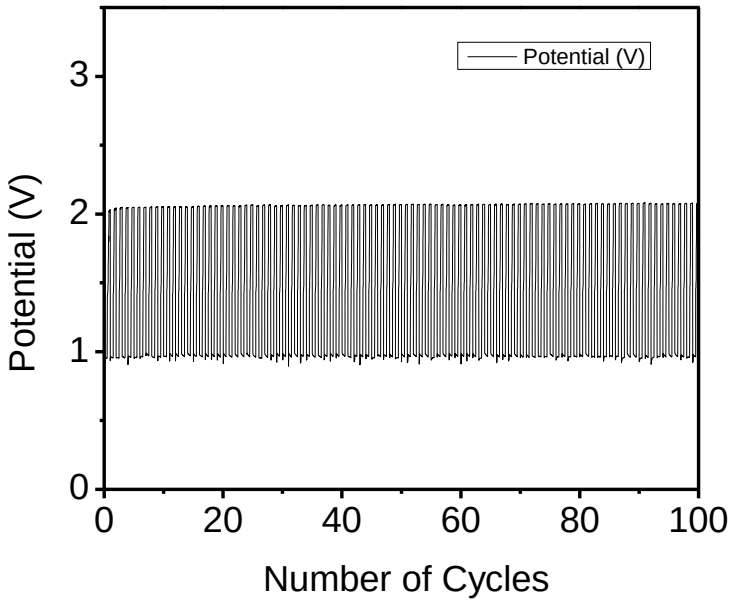

Figure 46: 400-500 cycles, cobalt oxide nanowires spray coated on stainless steel mesh gas diffusion layer

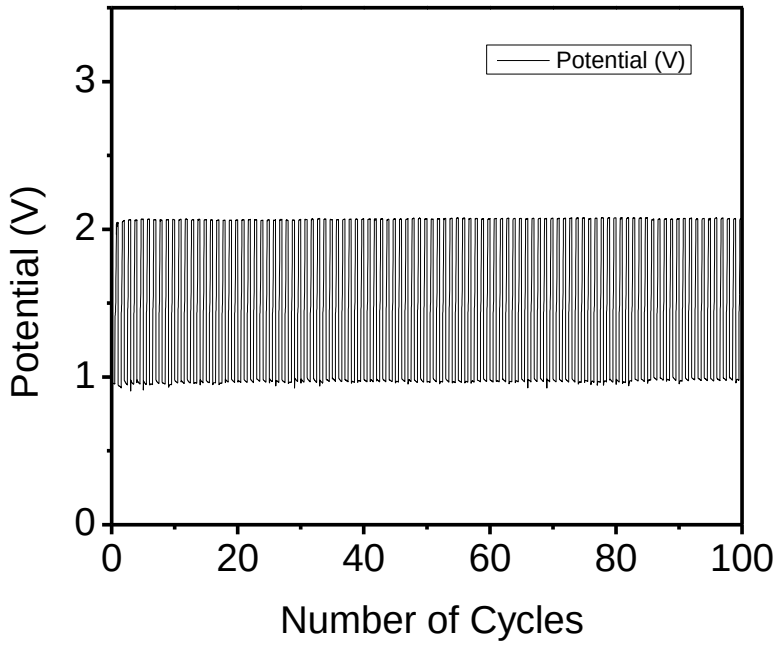

Figure 47: 500-600 cycles, cobalt oxide nanowires spray coated on stainless steel mesh gas diffusion layer

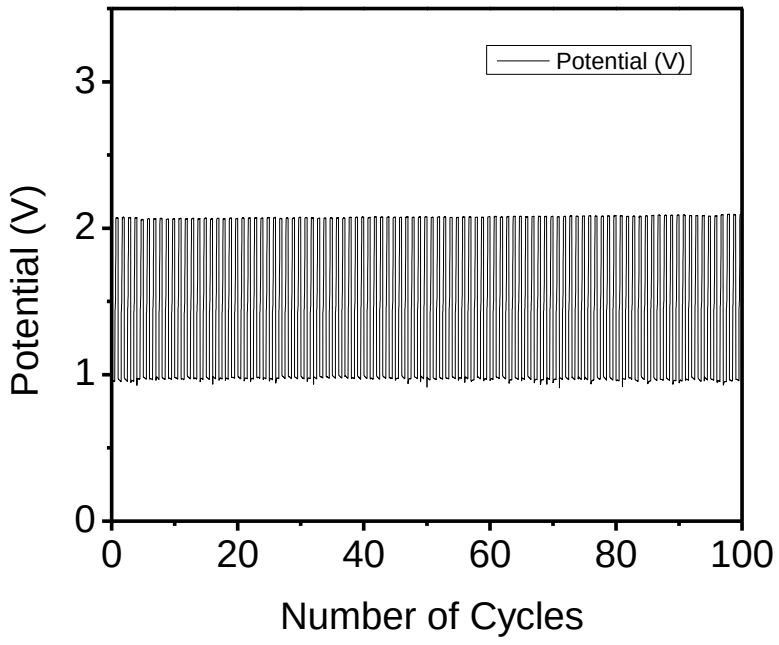

Figure 48: 600-700 cycles, cobalt oxide nanowires spray coated on stainless steel mesh gas diffusion layer

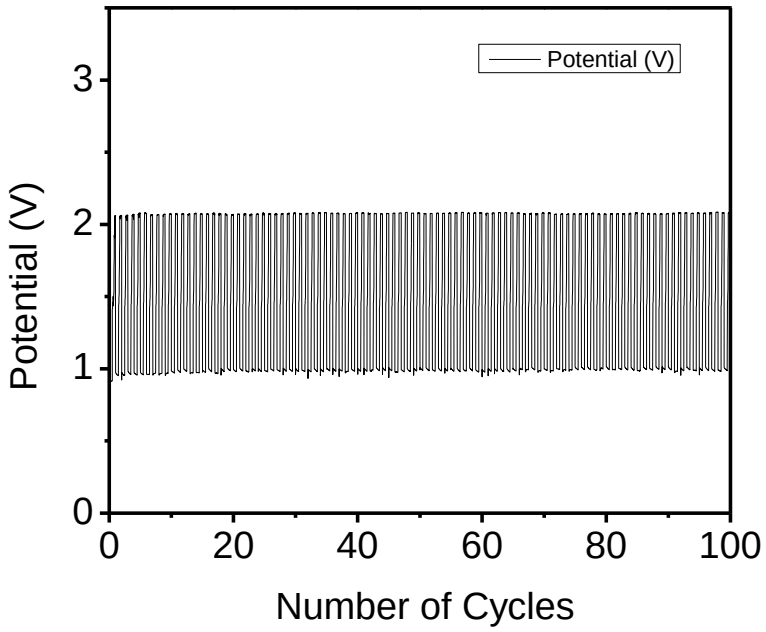

Figure 49: 700-800 cycles, cobalt oxide nanowires spray coated on stainless steel mesh gas diffusion layer

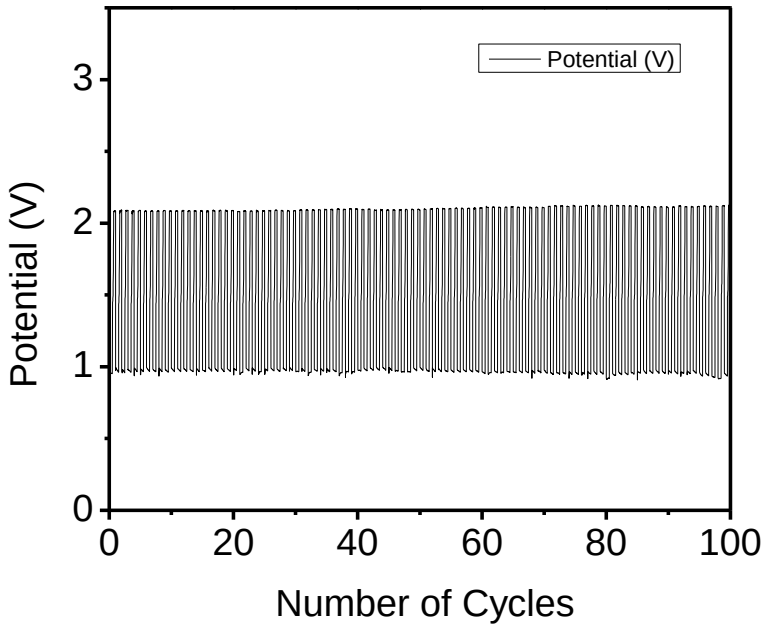

Figure 50: 800-900 cycles, cobalt oxide nanowires spray coated on stainless steel mesh gas diffusion layer

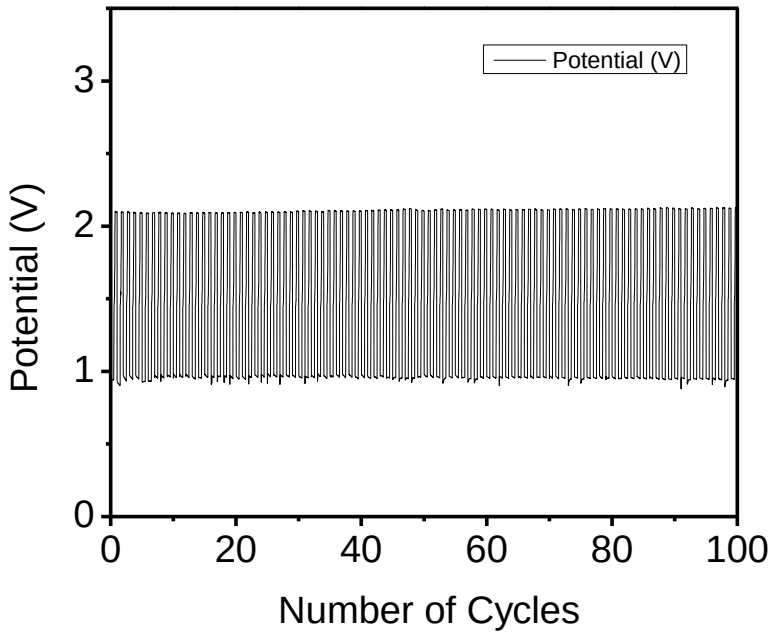

Figure 51: 900-1000 cycles, cobalt oxide nanowires spray coated on stainless steel mesh gas diffusion layer